# Structural exploration of a novel enzymatic hydration mechanism

Hamid-Reza Danesh-Azari

**MSc by Research**

University of York

Chemistry

January 2017

# Abstract

The enantioselective hydration of electron-rich C=C bonds is a synthetic challenge, particularly for the sustainable production of fine chemicals. Biocatalytic alternatives are developing, yet current options face limitations to their industrial application.

The enzyme Linalool Dehydratase-Isomerase (LDIase) enantioselectively adds water to myrcene in this way using a novel mechanism, further complemented by dehydration and isomerisation functions. This may not only bear a prospective biocatalytic tool for enantioselective hydration, but could also facilitate the manufacture of polymers from natural feedstocks.

To enable the application of LDIase as an industrial biocatalyst, this work further explored this enzyme's mechanistic details using structural studies. A 2.58 Å resolution structure of an LDIase mutant was obtained which gave an initial indicator of a covalent intermediate. An aerobic homologue was also investigated as a possible industrial alternative.

A comprehensive understanding of this enzymatic hydration mechanism will allow rational engineering of LDIase to expand its substrate range, for the diverse production of highly valuable chemicals. By this method, we may reduce our reliance on non-renewable petrochemical sources and energy-intensive synthesis to produce natural chemicals of higher quality.

# List of Contents

# List of Tables

# List of Figures

# Acknowledgements

I would like to sincerely thank Gideon Grogan for taking me on as a research student in his group. He has provided me with a quality of supervision I would be lucky to ever find again; allowing me to develop as an independent researcher, yet always generous with his time and assistance. Above all, I am indebted to him for giving me the opportunity to reignite my passion for science, and find work which I truly enjoy.

I would also like to thank the members of the Grogan group: Muhiadin Omar, my group brother; Amina Frese, my steadfast desk buddy; Tamara Mielke, for her inspirational spirit; Lilly Wells, for teaching me political philosophy and bravery; Henry Man, for his expertise; Laziana Ahmad, for her mirth; Mahima Sharma, for the friendly etymological discussions; and Anibal Cuetos Fernández, for always bringing a smile to my face. I have been privileged to have you as colleagues, but blessed to have you as friends.

I would also like to thank all the members of the York Structural Biology Laboratory for their endless help and community spirit. I would particularly like to thank Catherine Jardine and Jane Harrison for their administrative support; Simon Grist and Louise Haigh for their technical support; Tim Kirk for his computing support; and Johan Turkenburg and Sam Hart for X-ray support and crystal data collection.

My friends at York have made the last year an unforgettable one. You have all brought balance to my life, and through you I have experienced new and exciting things.

Finally, I would like to thank my parents for their endless love, guidance and selflessness. Without a doubt, you have made me who I am today.

# Author's Declaration

I declare that this thesis is a presentation of original work and I am the sole author. This work has not previously been presented for an award at this, or any other, University. All sources are acknowledged as References.

# Chapter 1.

## Introduction

### 1.1. Enantioselective hydration

#### 1.1.1. Water, the reactant

The hydration of alkenes is ubiquitous in nature, yet remains a laboured process for our own methods of chemical synthesis. Although the possession of lone pairs allows water to act as a nucleophile, its low electron density makes it a particularly weak one. This is exacerbated during water addition to electron-rich alkenes, where the reaction conditions can reduce water's electronegativity by protonating it.[1] Additionally, as water is both solvent and nucleophile, hydrogen bonding between molecules contributes to water's polar protic nature by reducing the availability of its lone pairs. Its excess as a solvent also leads to the position of equilibrium lying towards the starting material, which is less than ideal for producing industrially important chemicals. These factors do water few favours in appearing as an attractive reactant.

This being said, a reactant which is both exceptionally safe and in abundance on Earth is alluring, and many attempts have been made over the years to tap into the potential of hydration reactions.

The most widely-used hydration reaction today in the chemical industry is for the production of ethanol. Aside from fermentation, this can be accomplished by hydrating petrochemical-derived ethylene in steam using a phosphoric acid-based catalyst at high temperatures and high pressure.[2] The mechanism of this electrophilic addition, which uses acid catalysis, provides some insight into the challenges for the addition of water to electron-rich alkenes (***Figure 1.1***).

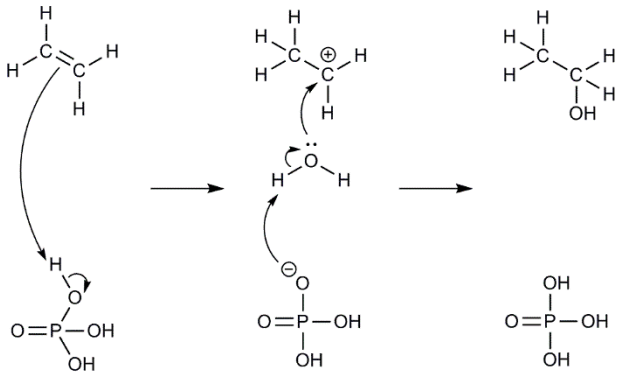

**Figure 1.1** Scheme of industrial ethylene hydration using steam and a phosphoric acid catalyst.

In this reaction, phosphoric acid acts as a Brønsted-Lowry acid, donating a proton to ethylene and forming a carbocation intermediate. Water carries out a nucleophilic attack of the protonated ethane, now a conjugate acid, to form an oxonium ion. In the final step this is deprotonated by the oxidised phosphoric acid to form ethanol and to regenerate the catalyst.

Another example of water addition to an electron-rich alkene is the hydration of isobutylene to form *tert*-butyl alcohol. This reaction occurs similarly to that of ethylene hydration, with the difference of occurring in the liquid phase under high pressure and using an acidic cation exchange resin.[3] However, unlike ethylene, isobutylene is an asymmetric alkene and therefore the location of carbocation formation affects the location of water addition (***Figure 1.2***). The Markovnikov Rule explains this issue; it states that the carbocation is most stable the more substituents it has. In practice, this means that hydrogen will be added to the carbon that is initially bound to the greatest number of hydrogens, and water will be added to the carbon which binds the fewest.

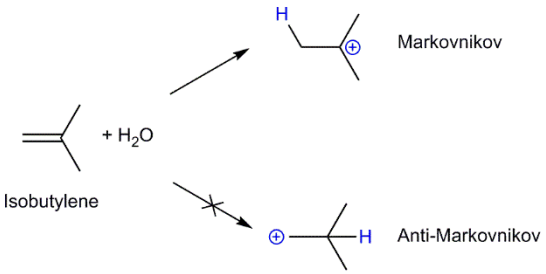


**Figure 1.2** Scheme demonstrating the Markovnikov Rule applied to isobutylene's carbocation intermediate of hydration.

Although both of these reactions show industrial applications of electron-rich alkene hydration, they are faced with a number of problems. The high temperatures and pressures required in these reactions increase costs, and this energy requirement coupled with the petrochemical source of the starting materials makes it environmentally unsustainable. Additionally, side reactions and dehydration of the product back to the starting material frequently occurs.[1] This is not only inefficient, but also reduces the purity of the desired chemical or requires additional workup steps. Although these processes are relatively straightforward for simple alcohols, they become much more difficult for more complex chemicals such as terpenes.

### 1.1.2. Enantioselectivity

Of all the problems described for industrial hydration, the most pressing is enantioselectivity. One of the ways in which chemicals increase in complexity is the possession of an asymmetric carbon, one bonded to four different groups. Compounds with these chiral centres exist as two enantiomers, (*R*)- or (*S*)-, which are mirrors of each other (***Figure 1.3***).

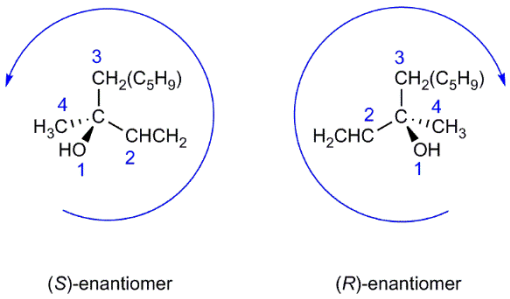


**Figure 1.3** The two enantiomeric assignments of linalool shown from a chiral-centric view, demonstrating CIP priority rules in blue.

Although the difference between such enantiomers can appear small when drawn, their real-world differences are stark. Nature itself shows favouritism; sugars are mostly D and amino acids L. The reason for this homochirality is not fully understood, however theories include the preferential destruction of single enantiomers by nuclear decay, or simply random chance.[4]

However, the relevance of enantiomers does not stop with their natural distribution. As nature shows favouritism in production, so does it in response; often only one enantiomer of a chemical will be physiologically active, but sometimes each enantiomer will induce contrasting effects. Scent is a good example of this, and our olfactory system can detect these subtle differences in chirality.[5] The flavour and fragrance industry is therefore particularly interested in scalable enantioselective synthesis.

Drugs are another example of this, even though for many enantiopurity is inconsequential. Ibuprofen (painkiller), cetirizine (antihistamine) and salbutamol (asthma) have been sold as racemic mixtures, even if a single enantiomer is preferentially active.[6] The primary reason for choosing enantiopurity in these instances would be efficiency of production. Yet drugs with enantiomers possessing different activities can have profound effects, such as the developmental effects of racemic thalidomide.[7]

Chemical synthesis struggles to achieve the same enantioselectivity achieved by nature. For the hydration of alkenes, several synthetic chemical attempts have been made; Vanderwal & Jacobsen developed an aluminium salen catalyst,[8] while Hartmann *et al.* opted for silicon- and boron-based complexes.[9] Boersma *et al.* took a different route with a DNA-based catalyst.[10] Although successful at introducing chirality, these catalysts were only demonstrated on electron-deficient enones. On the other hand, Ying Yan Jiang's group at the Chinese Academy of Sciences have used a wool-palladium complex to hydrate electron-rich carbon-carbon double bonds.[11,12]

These studies show that although synthetic chemistry solutions for the hydration of carbon-carbon double bonds do exist, they are applicable only to electron-deficient substrates or require rare metals and energy-intensive temperatures or pressures. Reactions of this kind are also frequently limited by low yields or poor enantiomeric excess. These factors make them a less than ideal solution to introducing chirality, and create an essential niche for catalysts which can enantioselectively hydrate electron-rich alkenes cheaply in an environmentally benign manner.

## 1.2. Biocatalysis

### 1.2.1. Life's catalyst

Mirroring the chirality of nature, life has evolved enzymes that perform enantioselective catalysis. The shape of an enzyme's active site precisely positions the substrate for specificity, while the location of catalytic amino acid residues controls selectivity.[13] This allows for chemo-, regio- and stereoselectivity, in addition to enantioselectivity. The precision with which enzymes control their reactions is necessary for ensuring side products are not formed, which can have potentially harmful physiological effects or undesired environmental consequences. Fortunately, these very properties also make enzymes an ideal tool for industry.

### 1.2.2. Man's biocatalyst

Our use of enzymes predates synthetic chemistry, having been exploited for millennia through fermentation for the conversion of sugars to alcohol. As our understanding of enzymes and their mechanisms has progressed, we have begun to use this natural tool for increasingly more advanced chemistry. Not only do enzymes boast the aforementioned specificity and selectivity, but their preference for mild conditions makes them much more environmentally benign than conventional chemical catalysts.[14]

Biocatalysis for important industrial reactions has been steadily increasing in recent years. In the flavour and fragrance industry the use of single enantiomers creates more realistic tastes and scents, while enzymatic production fulfils customers' increasing preference for natural products. In practice, the biotechnology companies Evolva and Oxford Biotrans have each developed an enzymatic technique for the manufacture of nootkatone, a chiral compound and principle contributor to grapefruit aroma (***Figure 1.4***).[15,16] Traditional methods of nootkatone extraction from grapefruit are expensive and difficult due to the $2.5 \times 10^{-4}$ % yield, however biocatalytic methods such as these provide a viable alternative which is being established for other flavour and fragrance chemicals.

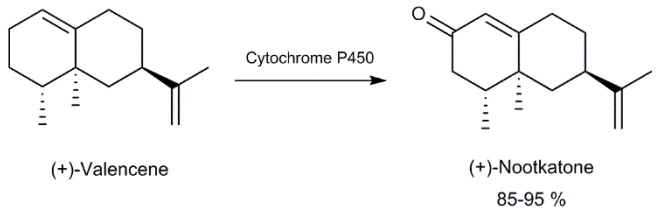


**Figure 1.4** Conversion of valencene to nootkatone, as catalysed by a cytochrome P450 enzyme.

Biocatalysis is also being applied to produce enantiopure pharmaceuticals. Ketoreductases are now an established route for the synthesis of chiral intermediates for atorvastatin to lower cholesterol,[17] and transaminases for the antidiabetic drug sitagliptin (***Figure 1.5***).[18] Complex drugs such as these often require multiple steps for their production, more of which now implement biocatalysts as the technology improves.[19]

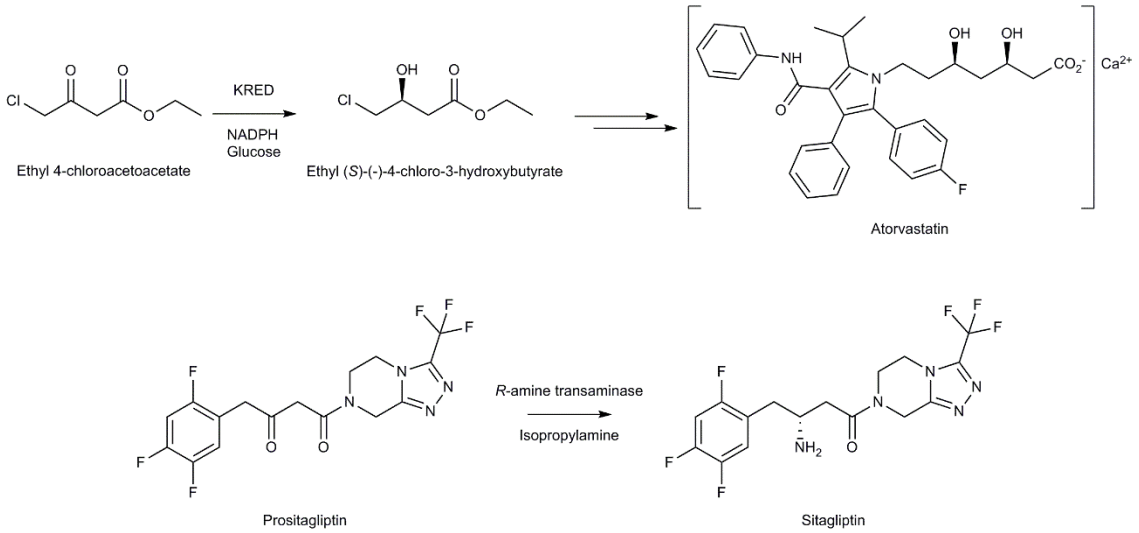


**Figure 1.5** Production of atorvastatin and sitagliptin precursors by biocatalysis, using either a ketone reductase or a transaminase respectively, introduces correct chiral centres to these drugs.

These modern biocatalytic reactions use isolated enzymes, which offer advantages in organic solvent tolerance and simpler product retrieval over whole-cells.[20] However, synthetic biology methods can engineer pathways for enzymatic cascades in whole-cells; a landmark example is artemisinin precursor production in yeast using cytochrome P450s, pioneered by Jay Keasling's group in collaboration with Amyris and Sanofi (***Figure 1.6***).[21–23]

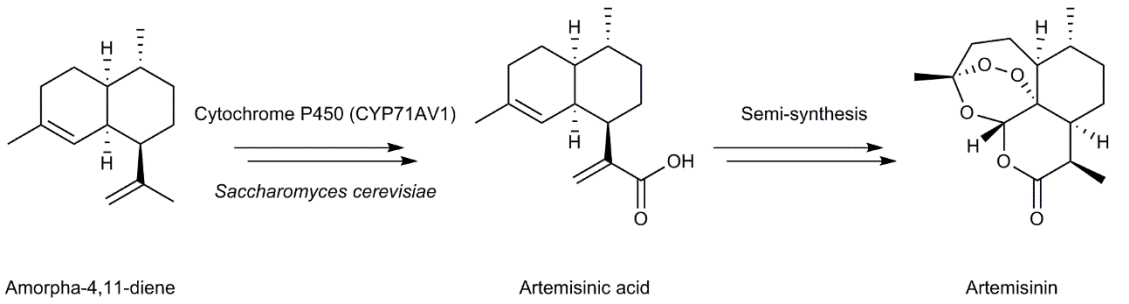


**Figure 1.6** An engineered biosynthetic mevalonate pathway of *S. cerevisiae* is complemented by the oxidation activity of a cytochrome P450 enzyme to produce the precursor of the antimalarial drug artemisinin.

As solutions to the formidable challenge of climate change become increasingly pressing, biocatalysis provides a potentially effective one. Its reduced environmental impact is not just important for reducing energy consumption and the reliance on toxic catalysts, but also by minimising our reliance on petrochemical sources. Many important polymers could only be made on an industrial scale from petroleum, but biocatalysis has facilitated production of partly bio-based polytrimethylene terephthalate (PTT) from dehydratase-fermented 1,3-propanediol (***Figure 1.7***).[24–26]

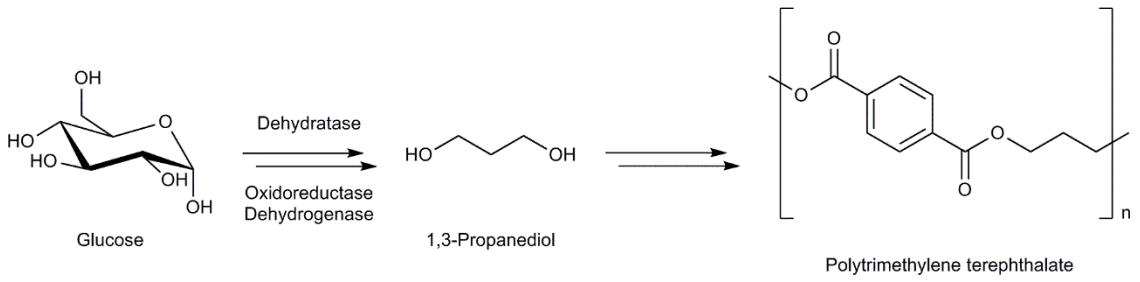


**Figure 1.7** 1,3-Propanediol (PDO) is catalysed from corn-derived glucose by three enzymes engineered into *E. coli*, replacing traditional petrochemical sources. This Bio-PDO is used to manufacture the PTT product Sorona (Du Pont).

As novel enzymes are discovered and their mechanisms fully understood, we can engineer biocatalysts to create affordable aromas, safe drugs and green materials.

## 1.3. Hydratases

Applying biocatalysis to alkene hydration provides another solution to the challenges of enantioselectivity faced by synthetic methods. There are currently a number of enzymes used industrially to accomplish this.

### 1.3.1. Fumarase

Fumarase is an enzyme essential in the citric acid cycle for the conversion of fumarate to (*S*)-malate, hydrating the central carbon-carbon double bond (***Figure 1.8***). This process contributes to the generation of the electron carrier NADH which is fed into the oxidative phosphorylation pathway to form ATP.

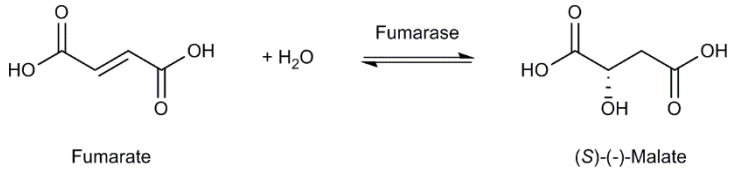


**Figure 1.8** Fumarase asymmetrically hydrates fumarate to (*S*)-malate in the citric acid cycle.

Two types of active site exist for fumarases; $Fe^{2+}$-dependent class I and cofactor-independent class II. Class I fumarases (FumA and FumB) use a [4Fe-4S] iron-sulfur cluster, where the non-protein bound iron is postulated to ligate both water and one of the carboxylate groups of the fumarate. Rather than forming a carbocation intermediate, this mechanism uses a covalent intermediate. This way, it increases proximal interactions to perform an intramolecular reaction. Here the iron acts as a Lewis acid catalyst, facilitating the reaction by increasing the electronegativity of its ligated carboxylate oxygen. Catalytic amino acid residues then separately accept a proton from bound water, and donate a proton to the carbon double bond (***Figure 1.9***).[27–29]

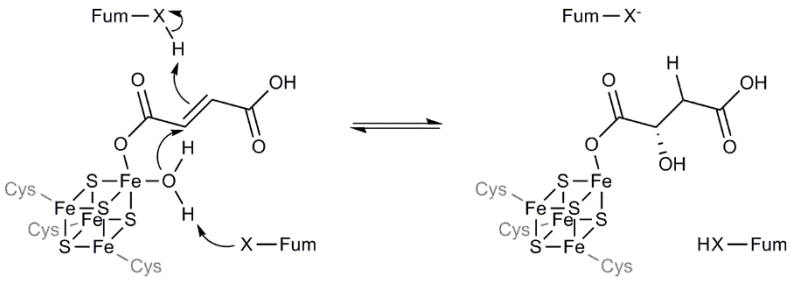


**Figure 1.9** Mechanism of fumarate hydration by the class I fumarase metalloenzymes. 'X' represents catalytic amino acids of the active site.

Class II fumarases (FumC) are homotetramers with four active sites each situated between three subunits, and an additional allosteric binding site.[30] Unlike class I fumarases they do

not possess an iron-sulfur cluster, so must utilise a different mechanism for hydration. This is accomplished by acid-base catalysis, with a protonated amino acid residue acting as an acid and a deprotonated residue acting as a base. The basic residue activates water by redistributing electron density towards oxygen for addition, while the acidic residue donates a proton to the $C_3$ carbanion (***Figure 1.10***). Which specific residues these are in fumarase is not fully known, however for fumarate hydration it is likely that the acid is serine and the base histidine.[31] Whether fumarate hydration or (*S*)-malate dehydration occurs depends on the protonation state of the amino acids.[32]

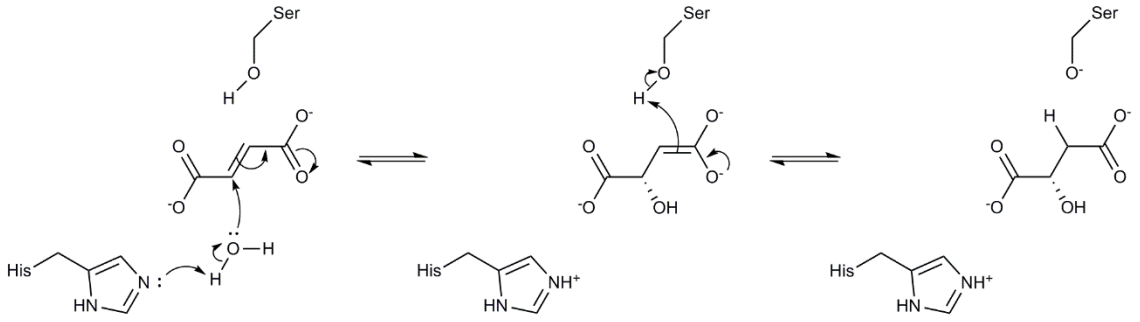


**Figure 1.10** Mechanism of fumarate hydration by class II fumarase.

The distinct mechanisms of enzymes which catalyse the same reaction raises the question of why this difference has evolved. It is suggested that the class I fumarases are utilised under anaerobic or microaerobic conditions, and class II is used in aerobic conditions where oxygen-sensitive metal cofactors would be inactivated.[33] This also applies to industry, where enantiopure (*S*)-malate is important for pharmaceuticals.[34] This has led to the use of class II fumarases in its production, for oxygen tolerance and stability at higher temperatures.[35]

### 1.3.2. Enoyl-CoA Hydratase

Enoyl-CoA hydratase, also known as crotonase and the namesake of the same superfamily, catalyses the hydration of *trans*-2-enoyl-CoA to 3-hydroxyacyl-CoA as part of the β-oxidation pathway (***Figure 1.11***). This process generates acetyl-CoA, which is supplied to the citric acid cycle of fumarase. The homohexameric protein is a dimer of trimers and has six active sites in total, each formed at the interface between two subunits.[36] The flexible active

site loop gives the enzyme a broad substrate spectrum, with chain lengths of trans-2-enoyl-CoA from four to twenty carbon atoms.[37]

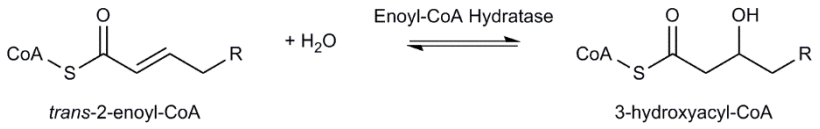


**Figure 1.11** Hydration reaction catalysed by enoyl-CoA hydratase in the β-oxidation pathway.

The proposed acid-base mechanism is likely to proceed by a carbanion intermediate, although a concerted transition state has also been suggested as a possibility.[38,39] Glutamate activates water for attack of the carbon-carbon double bond by the oxygen lone pair, forming the carbanion intermediate. This then abstracts the residual proton from glutamate to complete the reaction (***Figure 1.12***).

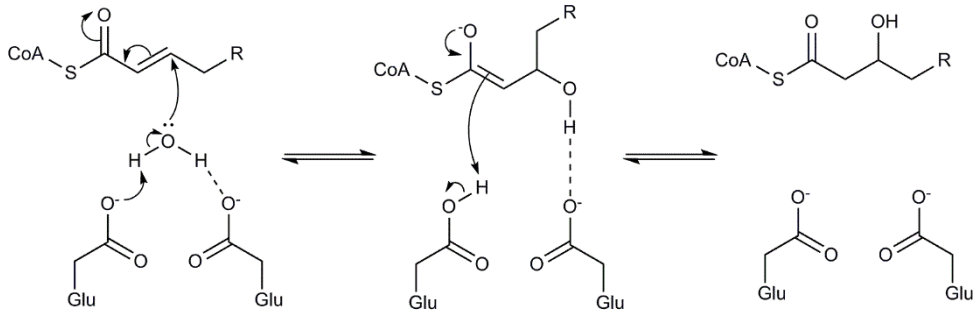


**Figure 1.12** Carbanion intermediate mechanism of enoyl-CoA hydratase, utilising a similar Michael addition to class II fumarase.

The oxyanion hole is particularly important for stabilisation of the carbanion intermediate, specifically in this instance glycine and alanine residues.[40] This particular enoyl-CoA hydratase catalyses the (*S*)-specific hydration, interestingly others carry out the (*R*)-specific reaction instead.[41] Eukaryotes often carry out the enoyl-CoA reaction in multifunctional enzymes, which have 3-hydroxyacyl-CoA dehydrogenase activity at one terminal domain and enoyl-CoA hydratase activity at the other, dependent on the enzyme.[42–44]

Enoyl-CoA hydratases can be used industrially to make 3-hydroxybutyrate for biopolyesters such as poly[(*R*)-3-hydroxybutyrate].[45] Similarly, 3-hydroxyisobutyric acid can be produced in a multi-enzyme pathway as a precursor for methacrylic esters such as poly(methyl methacrylate), which is also known by the trade name Perspex.[46] Enoyl-CoA

hydratase can serve in the adipate degradation pathway to adipyl-CoA to make precursors of the drug aminocaproic acid and the synthetic fibre polymer polycaprolactam.[47] For non-biocatalytic applications, enoyl-CoA is targeted by Henkel to reduce the unpleasant smell caused by 2-methylbutyric acid and isobutyric acid during the fermentation process for industrial detergent enzyme production.[48]

Although fumarase and enoyl-CoA are used industrially for carbon-carbon double bond hydration, their substrates are limited to enones using the Michael reaction. Although they provide a fascinating insight into the mechanism of hydration reactions, other enzymes will need to be explored to build biocatalytic tools for hydrating electron-rich alkenes.

### 1.3.3. Oleate Hydratase

Catalysing the hydration of the $C_{18}$ monounsaturated ω-9 fatty acid oleic acid to (*R*)-10-hydroxysteric acid (***Figure 1.13***), oleate hydratase was discovered in the soil bacterium *Pseudomonas*.[49] Structural studies on this enzyme have since caused a change in host name to *Elizabethkingia meningoseptica* and revealed a flavin-dependent monomeric enzyme.[50]

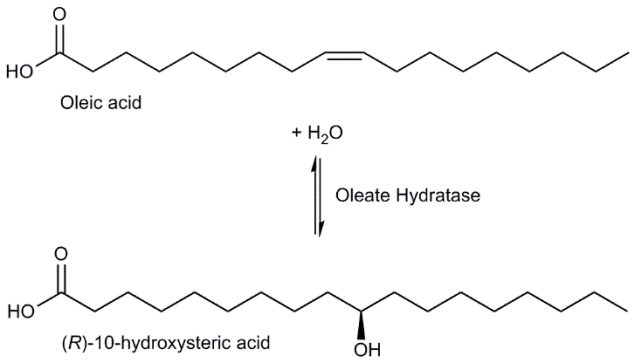


**Figure 1.13** (*R*)-selective water addition to oleic acid by oleate hydratase.

The mechanism employs acid-base catalysis, with amino acid residues glutamate and tyrosine playing a key role. The FAD cofactor is proposed to orient the substrate and stabilise the transition state. The glutamate residue activates the water similarly to mechanisms discussed previously, which in turn attacks the positive dipole of $C_{10}$ at the *re*-face. Finally, this carbon abstracts a proton from tyrosine (***Figure 1.14***).[51]

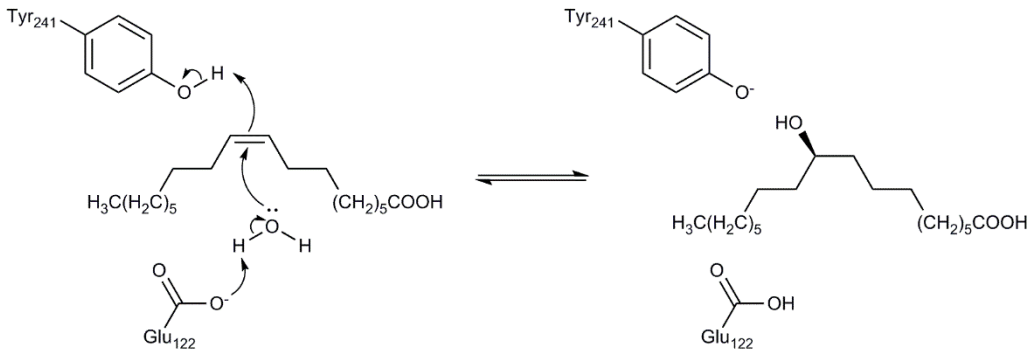


**Figure 1.14** Hydration mechanism of oleate hydratase. An FAD cofactor is utilised by the enzyme (not shown).

The production of (*R*)-10-hydroxysteric acid using oleate hydratases is industrially applied by the flavour industry for the production of γ-dodecalactone, which contributes to the flavour of whiskey.[52–54]

### 1.3.4. Carotenoid 1,2-Hydratase

Carotenoid hydratases have been discovered in two forms; CrtC from photosynthetic bacteria and CruF from a non-photosynthetic bacterium.[55] Both terminally hydrate long, highly unsaturated $C_{40}$ hydrocarbon carotenes; CrtC catalyses lycopene to 1-HO-lycopene then 1,1'-$(HO)_2$-lycopene (***Figure 1.15***), whilst CruF hydrates γ-carotene.

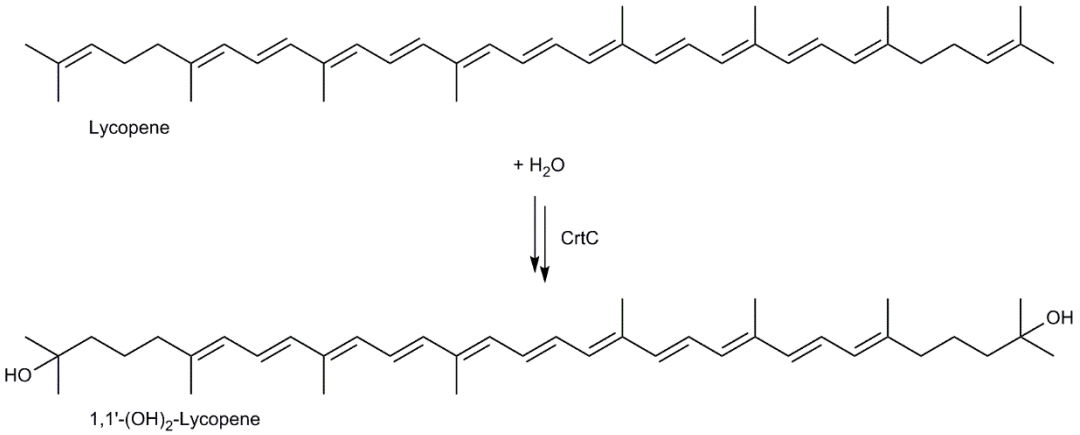


**Figure 1.15** The carotenoid 1,2-hydratase CrtC can hydrate each end of lycopene consecutively.

No structure is available for this class of hydratase, though a mechanism has been suggested for CrtC using a homology model.[56] The proposed mechanism is by acid-base catalysis, with an aspartate residue acting as the acid, with its acidity enhanced by a neighbouring

histidine and bridged to tyrosine by a water molecule (supplementary online text).[56] The elucidation of a structure, ideally as a Michaelis complex, would shed light on this mystery.

Although enzymes exist for the hydration of electron-rich carbon-carbon bonds, there are few which are well characterised. New enzymes with novel mechanisms are essential for the industrial implementation of this promising biocatalytic tool, such as for the production of monoterpenes.

## 1.4. Terpenes

Terpenes are unsaturated hydrocarbon derivatives of isoprene, their molecular building block. This class of natural organic compounds have strong aromas and are primarily released by plants for defence or cloud-seeding, and by some insects.[57] Humans best know them for their strong and pleasant aromas as natural essential oils, and are found in the majority of perfumes, cosmetics and personal care products. They have become a cornerstone of the fragrance industry, but are also rapidly becoming an essential source of new drugs such as artemisinin.

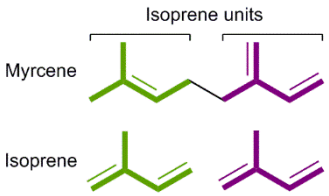


**Figure 1.16** The isoprene rule as demonstrated using myrcene. Individual isoprene units are coloured separately, with the isoprene backbones in bold.

Terpenes exist in a variety of classes, based on the isoprene rule of $(C_5H_8)_n$ where n represents the number of isoprene units connected by a carbon-carbon bond (***Figure 1.16***). The isoprene rule can also be applied to compounds we often have different associations with; for example, Vitamin A is a terpene. Selected terpene classes are shown in ***Table 1.1***.

**Table 1.1** Representative terpene classes, displaying the number of isoprene units, the molecular formula, and notable examples. The monoterpenes also include linalool and geraniol.

| Class | Isoprene units | Molecular formula | Examples |
|---|---|---|---|
| Hemiterpenes | 1 | C5H8 | Isoprene |
| Monoterpenes | 2 | C10H16 | Pinene, Limonene, Myrcene |
| Sesquiterpenes | 3 | C15H24 | Farnesol, Humulene |
| Diterpenes | 4 | C20H32 | Taxadiene |
| Triterpenes | 6 | C30H48 | Squalene |
| Tetraterpenes | 8 | C40H64 | Lycopene |
| Polyterpenes | *n* | | Natural rubber |

Monoterpenes are one such class, and are one of the most common terpenes used for their bright scents. Below we will discuss three of these monoterpenes; myrcene, geraniol, and linalool, and how they are currently industrially synthesised and employed.

### 1.4.1. Myrcene

Myrcene exists as two isomers, α-myrcene and β-myrcene; it is the latter which occurs naturally (***Figure 1.17***). β-myrcene is a colourless oil with a sharp herbal scent, and makes a considerable contribution to the aroma of hops.[58]

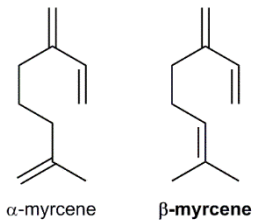


**Figure 1.17** The two constitutional isomers of myrcene. Only β-myrcene exists in nature (bold).

A strain of *Rhodococcus erythropolis* has been isolated from the soil of hop plants which catalyses β-myrcene to geraniol.[59] For the industrial production of myrcene, turpentine is used; a distillate of pine trees containing α- and β-pinene. The latter undergoes pyrolysis to

break the bicyclic ring, forming myrcene. Although theoretical yields could be as high as 93.5%, the maximum reported yields are 85%.[60]

### 1.4.2. Geraniol

Geraniol, or *trans*-3,7-dimethyl-2,6-octadien-1-ol, is widely used as a fragrance in many consumer products including soaps and perfumes (***Figure 1.18***). It carries a fresh, citrus scent and is a key constituent in the essential oils of rose, lemongrass and palmarosa.[61] Nerol is the *cis*-isomer of geraniol, with a similar yet distinct aroma.

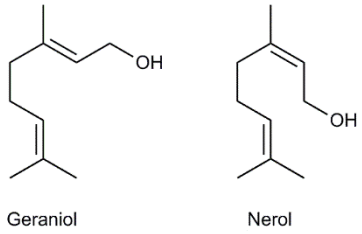


**Figure 1.18** The *cis-trans* stereoisomers geraniol (*trans*) and nerol (*cis*).

Fractional distillation of these essential oils yields high-purity natural geraniol, though industrial chemistry can produce it synthetically. This can include the selective hydrogenation of petrochemically-derived citral and distillation using ruthenium-iron or platinum-zinc oxide catalysts.[62,63] BASF is one such company which has purpose-built facilities to carry out this reaction on an industrial scale.

### 1.4.3. Linalool

Whereas myrcene exists as two constitutional isomers and geraniol has a configurational isomer, linalool is chiral at $C_3$ and thus has two enantiomers; (*S*)-(+)-linalool and (*R*)-(-)-linalool (***Figure 1.19***). By chemical nomenclature it is known as 3,7-dimethylocta-1,6-dien-3-ol.

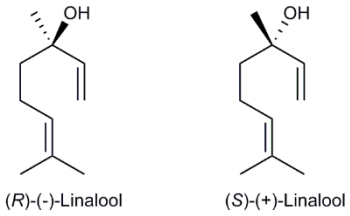


**Figure 1.19** Enantiomers of linalool, with both found in nature.

Unusually for a chiral compound, linalool is found in nature as both of its possible enantiomers. (*R*)-linalool is known as licareol and is described as having a woody, lavender-like aroma. (*S*)-linalool, or coriandrol, gives a difference scent illustrated as sweet, floral and citrusy.[64]

This substantial difference in scent creates a problem for the flavour and fragrance industry, which widely uses linalool in 61-97% of household products and cosmetics.[65] Natural extraction provides control over this disparity, however yields are low.[66] Current methods for industrial production involve semisynthesis of pinene, or organic synthesis of 2-methyl-2-hepten-6-one.[64]

However, this racemic linalool does not hold the desired aroma of a single enantiomer, and thus cannot evoke the same recognition of the scents we experience in our environment.[67] Instead, they take on an artificial 'chemical' smell; undesirable for selling fragranced products.

Approaching linalool synthesis as nature does may help alleviate this issue. Plants employ a variety of linalool synthases to make linalool enantioselectively, however for industrial application feedstock price and availability must be taken into account.[68] A practical alternative is utilising biotechnology for this purpose, such as microbial transformations, synthetic biology and biocatalysis.[69,70]

With the cost of natural product extraction of valuable terpenes remaining high while demand continues to increase, industry must rely on synthetics. However, this presents additional challenges in enantioselectivity. The use of modern biotechnological techniques

such as biocatalysis can solve both of these issues by creating 'naturally' formed products that are also enantiopure.

## 1.5. Linalool Dehydratase-Isomerases

### 1.5.1. *C. defragrans* Linalool Dehydratase-Isomerase (LDIase)

Linalool Dehydratase-Isomerase, named LDIase, was discovered in *Castellaniella defragrans*, previously known as *Alcaligenes defragrans*.[71–73] This enzyme was shown to catalyse the reversible hydration of myrcene to geraniol via (*S*)-linalool (***Figure 1.20***).[74] As the equilibrium of this reaction lies towards myrcene the enzyme was named dehydratase rather than hydratase, and its ability to isomerise linalool to geraniol supplied the last part of its name.

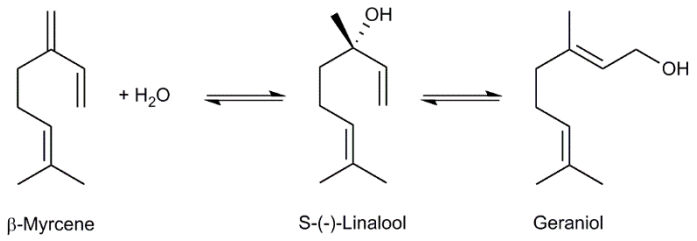


**Figure 1.20** The reversible hydration and isomerisation reactions catalysed by the enzyme Linalool Dehydratase-Isomerase (LDIase) from *C. defragrans*. Dehydration from geraniol is favoured.

This enzyme's ability to enantioselectively hydrate the electron-rich carbon-carbon double bond of myrcene make it an attractive enzyme to study in an underpopulated class. Since myrcene is readily found in hops grown abundantly for the brewing industry, this enzyme could potentially produce a valuable fragrance from an inexpensive feedstock.

Recent work in the Grogan group has solved the structure of this enzyme with geraniol (***Figure 1.21***), and suggests either a covalent or carbocation intermediate acid-base catalysed reaction for the dehydration of linalool to myrcene or its isomerisation to geraniol (***Figure 1.22***).[75] However, the mechanism of its unique enantioselective hydration of myrcene to (*S*)-linalool and isomerisation of geraniol to the same requires further investigation, specifically how it is able to introduce chirality.

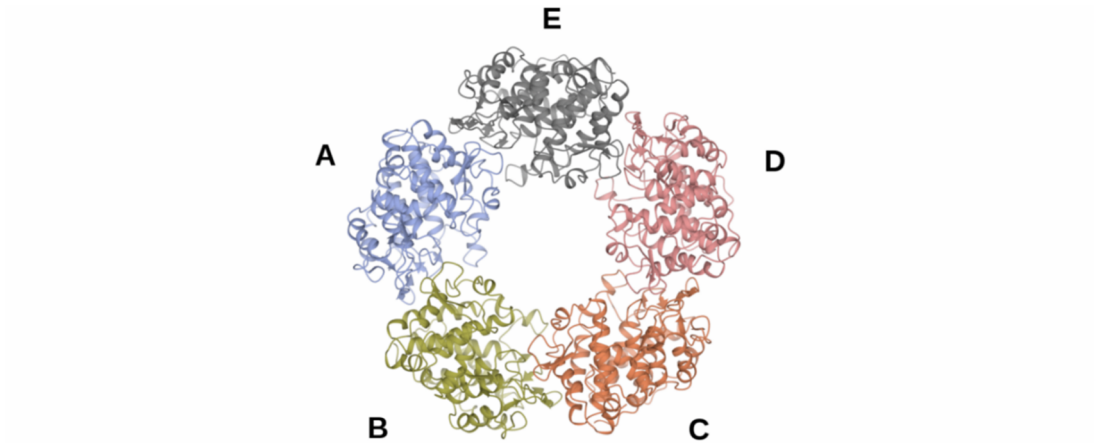


**Figure 1.21** X-ray crystallographic structure of the LDIase pentamer, with molecules of the asymmetric unit labelled.

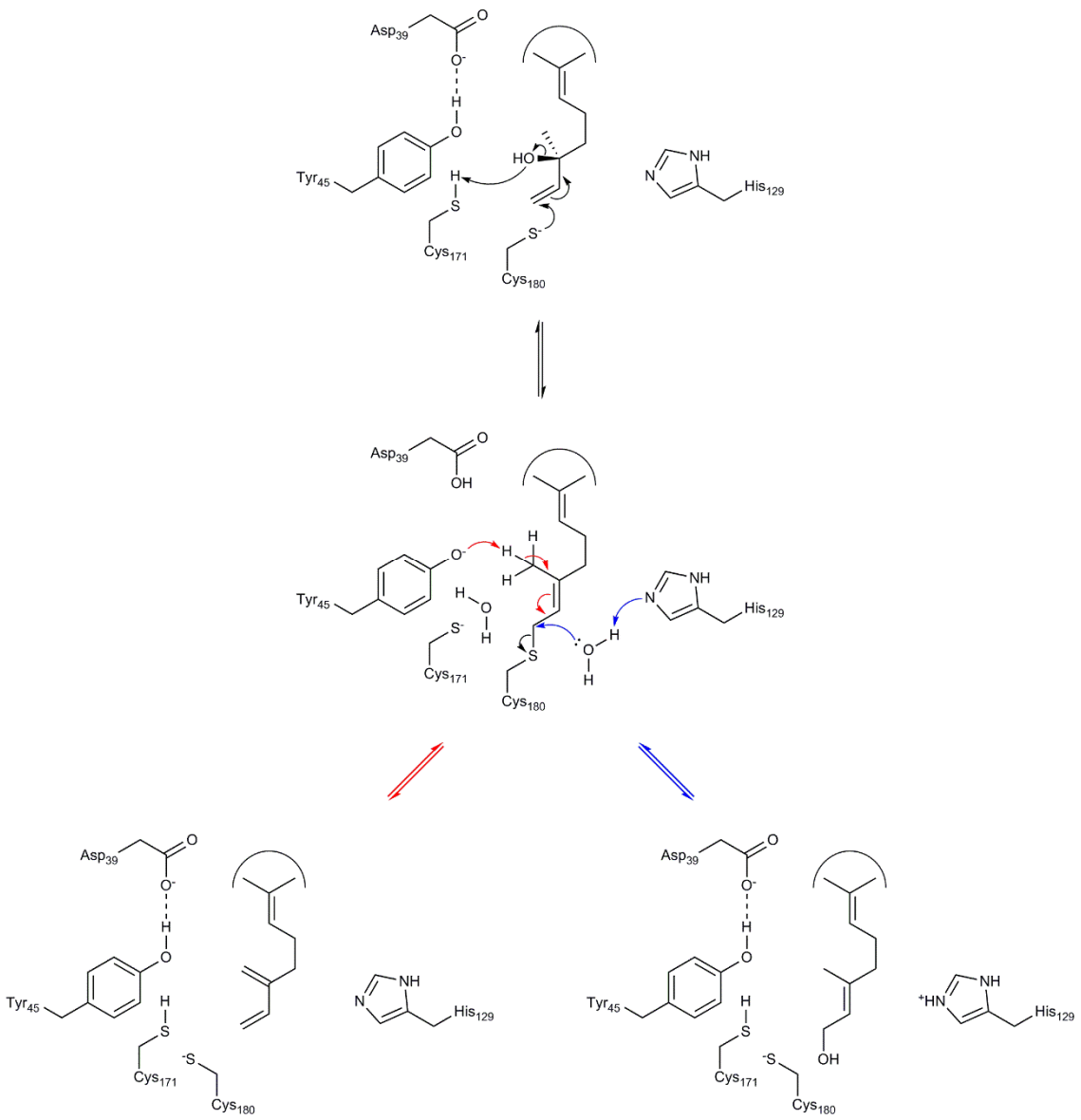


**Figure 1.22** Scheme of proposed covalent LDIase mechanism for the dehydration and isomerisation of linalool. Arrows in red indicate dehydration, and arrows in blue isomerisation. The mechanism of hydration can be deduced by following the reaction in reverse.

A full understanding of this reaction mechanism would allow for the rational design of this enzyme to improve its enantiomeric excess and, importantly, to increase substrate range. Patents have been filed which describe the random engineering of LDIase, allowing it to dehydrate crotyl alcohol to 1,3-butadiene and isoprenol to isoprene.[76–78] The polymers of these subunits are the main components of natural and synthetic rubber, providing a potentially petrochemical-free way of making incredibly valuable products.[79,80]

### 1.5.2. *R. erythropolis* Linalool Dehydratase-Isomerase (ReLDIase)

Although LDIase has demonstrated the excellent ability to catalyse an important industrially useful reaction, it faces possible issues with oxygen-sensitivity.[71] *R. erythropolis* was found by Thompson *et al.* to catalyse the same reaction as LDIase, though before the publication of the latter.[59] The benefit of this is that *R. erythropolis* does not face these issues, and identification of a linalool dehydratase-isomerase homologue would provide a prospectively more industrially-applicable enzyme for biocatalysis. Heterologous expression, purification and crystallisation for structure solution would also confirm the enzymes' similarities and any novel mechanistic features.

## 1.6. Project aims

The aims of this project are as follows:

I. The expression, purification, and co-crystallisation of LDIase with linalool to structurally determine a Michaelis complex of the intermediate transition state.

II. Mutagenesis studies of residues suspected to be essential in the catalytic mechanism, namely C171. Mutation of this residue to a serine could create a slow mutant, which can be structurally studied for a clearer understanding of the enzyme mechanism.[81]

III. The heterologous expression in *E. coli* using the pET-YSBLIC3C vector of the linalool dehydratase-isomerase homologue from *R. erythropolis*, putatively named ReLDIase, to determine an aerobic alternative to LDIase for industrial application.

# Chapter 2.

## Experimental Methods

### 2.1. Materials

#### 2.1.1. Chemicals

Chemicals were purchased from Fisher Scientific UK, Fluka Chemie GmbH, Formedium Ltd., Melford Biolaboratories Ltd., Merck KGaA, National Diagnostics, Sigma-Aldrich LLC, or VWR International bvba unless stated otherwise.

Crystallisation screens were purchased from Hampton Research (Index HT) or Molecular Dimensions (PACT *premier* and CSS I & II).

Restriction enzymes, agarose gel dyes, and agarose gel ladders were supplied by New England Biolabs (NEB).

The majority of water used in this work is UPW, for type I ultrapure (> 18 MΩ·cm).

#### 2.1.2. Plasmids

Gene for *Rhodococcus erythropolis* Linalool Dehydratase-Isomerase (ReLDIase) of 1698 bp was synthesised by Invitrogen (GeneArt) and hosted in the pMK-RQ (kanR) vector.

The vector used for introduction of a cleavable N-terminal hexahistidine tag to genes of interest was pET-YSBLIC3C, a derivative of pET-28a, provided in-house.

#### 2.1.3. Primers

Primers were synthesised by Eurofins Genomics, purified by HPSF (High Purity Salt Free) and provided in lyophilised format.

Primers designed for LDIase mutagenesis are described in ***Table 2.1***.

**Table 2.1** Primers for C171S site-directed mutagenesis of LDIase by QuikChange. The positions of mutated nucleotides are highlighted in red.

| Primer name | $T_m$ / °C | DNA sequence (5′ → 3′) |
|---|---|---|
| LDI_C171S_FOR | 75.1 | CCGTTTGCCGGTATTGTTAGCGAACCGGATAACTATTTTG (40) |
| LDI_C171S_REV | 75.1 | CAAAATAGTTATCCGGTTCGCTAACAATACCGGCAAACGG (40) |
| LDI_t511a_FOR | 79.45 | GCAAATCCGTTTGCCGGTATTGTTAGTGAACCGGATAA (38) |
| LDI_t511a_REV | 79.45 | TTATCCGGTTCACTAACAATACCGGCAAACGGATTTGC (38) |

Primers designed for ReLDIase LIC-based molecular cloning are described in ***Table 2.2***.

**Table 2.2** Primers for LIC cloning of ReLDIase into pET-YSBLIC3C. The pET-YSBLIC3C complementary regions are highlighted in yellow, and the gene insert complementary regions in cyan.

| Primer name | $T_m$ / °C | DNA sequence (5′ → 3′) |
|---|---|---|
| ReLDI_F_LIC3C | > 75 | CCAGGGACCAGCAATGAGCAGCATTAGCCGTCGTAGCCTG (40) |
| ReLDI_R_LIC3C | > 75 | GAGGAGAAGGCGCGTTAGGTCCATTTCAGGGTCACGGTGGTG (42) |

Primer designed for ReLDIase signal peptide cleavage is described in ***Table 2.3***.

**Table 2.3** Primers for LIC cloning of ReLDIase into LIC3C, removing 81 N-terminal nucleotides (27 amino acids) to create ReLDI-27ase. The pET-YSBLIC3C complementary regions are highlighted in yellow, and the gene insert complementary regions in cyan.

| Primer name | $T_m$ / °C | DNA sequence (5′ → 3′) |
|---|---|---|
| ReLDI-81_FOR | > 75 | CCAGGGACCAGCAATGAGCGCATGTAGCACCGCAACCACC (40) |

### 2.1.4. Growth media

Growth media used for transformation include Super Optimal Broth (SOC) and NZY$^+$, the former was supplied with chemically competent cells. Lysogeny Broth (LB) was used for both inoculation of starter cultures and in some expression experiments. Minimal Medium M9 was used for expression tests. Terrific Broth (TB) was used for the majority of large-scale expression.

Water used in the preparation of all media is referred to as UPW, for type I ultrapure (> 18 MΩ·cm).

All autoclaving was carried out at 121 °C for 20 min.

NZY$^+$ Media

| | |
|---|---|
| NZ amine (casein hydrolysate) | 2.0 g |
| Yeast extract | 1.0 g |
| Sodium chloride (NaCl) | 1.0 g |
| UPW | 200 mL |
| → autoclaved | |
| 1 M $MgCl_2$* | 2.5 mL |
| 1 M $MgSO_4$* | 2.5 mL |
| 20 % w/v Glucose* | 4 mL |

*addition after autoclaving step, carried out under aseptic conditions by filtration with a 0.22 μm membrane.

Adjustment of pH to 7.5 prior to autoclaving. Final composition divided into 1 mL aliquots for storage at -20 °C.

Minimal Medium M9

| | |
|---|---|
| Sodium phosphate dibasic ($Na_2HPO_4$) | 6.0 g |
| Potassium phosphate monobasic ($KH_2PO_4$) | 3.0 g |
| Sodium chloride (NaCl) | 0.5 g |
| Ammonium chloride ($NH_4Cl$) | 1.0 g |
| UPW | 1000 mL |
| → autoclaved | |
| 1 M Magnesium sulfate ($MgSO_4$)* | 1 mL |
| 0.1 M Calcium chloride ($CaCl_2$)* | 1 mL |
| 10 % w/v Glucose* | 10 mL |

*addition after autoclaving step, carried out under aseptic conditions by filtration with a 0.22 μm membrane.

Lysogeny Broth (LB) Media

| | |
|---|---|
| Sodium chloride (NaCl) | 10.0 g |
| Tryptone | 10.0 g |
| Yeast extract | 5.0 g |
| UPW | 1000 mL |
| → autoclaved | |

Terrific Broth (TB) Media

| | |
|---|---|
| Yeast Extract | 24.0 g |
| Tryptone | 12.0 g |
| Glycerol | 4 mL |
| UPW | 900 mL |
| → autoclaved | |
| Phosphate Salts* | 100 mL (10 % of total volume) |

*addition after autoclaving step, carried out under aseptic conditions using sterile equipment.

Phosphate Salts

| | | |
|---|---|---|
| Potassium phosphate dibasic ($K_2HPO_4$) | 87.8 g | 0.72 M |
| Potassium phosphate monobasic ($KH_2PO_4$) | 16.2 g | 0.17 M |
| UPW | 700 mL | |
| → autoclaved | | |

### 2.1.5. Buffers

#### 2.1.5.1. Protein purification buffers

Three buffers were used for cell lysis and purification, and each has been assigned a signifier name to explain its purpose. Buffer A is the 'Cell' buffer, used for cell pellet resuspension and

to hold lysate. For these purposes it contains glycerol to maintain cell and protein stability, and imidazole to prevent non-specific protein binding during the nickel column loading step. Buffer B is the 'Protein' buffer, which contains no imidazole and is used as the major protein-holding liquid. Buffer C is the 'Imidazole' buffer, which contains a very high (500 mM) concentration of imidazole to elute histidine-tagged, column-bound protein during IMAC purification by competing for the nickel immobilised to the resin.

All three buffers were pH adjusted to 8.0, then vacuum filtered at 0.22 μm and degassed.

Buffer A 'Cell'

| | | |
|---|---|---|
| Sodium chloride (NaCl) | 500 mM | 14.6 g |
| Tris | 50 mM | 3.0 g |
| Imidazole (low-UV) | 20 mM | 0.7 g |
| Glycerol | 10 % | 50 mL |
| UPW | | 500 mL |

Buffer B 'Protein'

| | | |
|---|---|---|
| Sodium chloride (NaCl) | 500 mM | 29.2 g |
| Tris | 50 mM | 6.0 g |
| UPW | | 1000 mL |

Buffer C 'Imidazole'

| | | |
|---|---|---|
| Sodium chloride (NaCl) | 500 mM | 29.2 g |
| Tris | 50 mM | 6.0 g |
| Imidazole (low-UV) | 500 mM | 34.0 g |
| UPW | | 1000 mL |

#### 2.1.5.2. Electrophoresis buffers

Tris-acetate-EDTA (TAE) Buffer (50x)

| | | |
|---|---|---|
| Tris | 242 g | 10 mM |
| Acetic acid glacial | 57 mL | 1 mM |
| EDTA (0.5 M, pH 8.0) | 100 mL | 50 mM |

| | | |
|---|---|---|
| UPW | | to 1 L |

Adjustment of pH to 7.5

SDS-PAGE Resolving Buffer

| | | |
|---|---|---|
| Tris | 1.5 M | pH 8.8 |
| SDS | 10 % | |

SDS-PAGE Stacking Buffer

| | | |
|---|---|---|
| Tris | 0.5 M | pH 6.8 |
| SDS | 0.4 % | |

SDS-PAGE Running Buffer Stock (4x)

| | |
|---|---|
| Glycine (electrophoresis grade) | 115.2 g |
| Tris | 24.0 g |
| UPW | 2000 mL |

SDS-PAGE Running Buffer

| | |
|---|---|
| SDS-PAGE Running Buffer Stock (4x) | 250 mL |
| UPW | 750 mL |
| 10 % (w/v) SDS | 10 mL |

SDS-PAGE Sample Loading Buffer (2x)

| | |
|---|---|
| SDS-PAGE Stacking Buffer | 1.2 mL |
| 50 % (w/v) Glycerol | 2.0 mL |
| 10 % (w/v) SDS | 2.0 mL |
| 1 % (w/v) Bromophenol blue | 0.5 mL |
| β-mercaptoethanol | 0.5 mL |
| UPW | 3.8 mL |

## 2.2. Mutagenesis

### 2.2.1. Primer design

Primers for mutagenesis were designed according to the requirements specified by the QuikChange Site-Directed Mutagenesis method.

Primers LDI_C171S_FOR and LDI_C171S_REV were designed using the PrimerX primer design tool, selecting 'QuikChange Site-Directed Mutagenesis Kit by Stratagene' at step 4 and 'Escherichia coli' at step 6 with default parameters.

Primers LDI_t511a_FOR and LDI_t511a_REV were designed using the Agilent QuikChange Primer Design Program, selecting 'QuikChange' at step 2.

### 2.2.2. PCR using PfuTurbo DNA polymerase

PfuTurbo DNA polymerase (Agilent) was used for mutagenesis due to its high fidelity and ability to extend long DNA. A PCR reaction mixture of 50 µL was assembled as described in ***Table 2.4***. $Mg^{2+}$ was not added separately to the reaction mixture as it was present in the buffer.

**Table 2.4** PfuTurbo PCR reaction mixture.

| Component | Stock Concentration | Volume / µL |
|---|---|---|
| Autoclaved UPW | | 36 |
| Cloned Pfu reaction buffer | 10x | 5 |
| dNTPs | 2 mM each nucleotide | 5 |
| DNA template (plasmid) | ≥ 100 ng $\mu L^{-1}$ | 1 |
| Forward primer | 20 pmol $\mu L^{-1}$ | 1 |
| Reverse primer | 20 pmol $\mu L^{-1}$ | 1 |
| PfuTurbo DNA polymerase | 2.5 U $\mu L^{-1}$ | 1 |

Thermocycling parameters were set as described in ***Table 2.5*** using a Bioer LifeECO thermal cycler.

**Table 2.5** PfuTurbo PCR thermocycling parameters.

| Segment | Cycles | Temperature / °C | Time / s |
|---|---|---|---|
| Initialisation | 1 | 95 | 300 |
| Denaturation | 18 | 95 | 60 |
| Annealing | | 55 | 60 |
| Elongation | | 72 | 60 $kb^{-1}$ |
| Final elongation | 1 | 72 | 300 |
| Cooling | 1 | 4 | 120 |
| Hold | | 10 | ∞ |

### 2.2.3. Touchdown PCR

Touchdown PCR was used as a possible solution to the difficulties associated with high primer melting temperatures, such as poor template annealing and primer-dimer formation.[82] The PCR reaction mixture was assembled as described in ***Table 2.4*** *ut supra*. Thermocycling parameters were set as described in ***Table 2.6***.

**Table 2.6** Touchdown PCR thermocycling parameters.

| Segment | Cycles | Temperature / °C | Time / s |
|---|---|---|---|
| Initialisation | 1 | 95 | 120 |
| Denaturation | 15 | 95 | 30 |
| Annealing | | 72* | 30 |
| Elongation | | 72 | 60 $kb^{-1}$ |
| Denaturation | 20 | 95 | 30 s |
| Annealing | | 64 | 30 s |
| Elongation | | 72 | 60 $kb^{-1}$ |
| Final elongation | 1 | 72 | 600 |
| Cooling | 1 | 4 | 120 |
| Hold | | 10 | ∞ |

*decreases by 0.5 °C each cycle

### 2.2.4. Digestion of parental plasmid DNA with DpnI

To prevent the subsequent transformation of non-mutated parental plasmid DNA used as a template in the PCR reaction, DpnI was used to digest this *E. coli*-derived and thus methylated DNA.

After thermocycling, 1.5 μL DpnI (2 units $\mu L^{-1}$) was added to the PCR reaction mixture. The digest reaction was incubated at 37 °C for 4.5 hours.

### 2.2.5. Transformation, DNA isolation and sequencing

DpnI-digested DNA was transformed into E. coli XL10-Gold cells as in [***2.4***], but with addition of 5 μL DNA.

Mutated plasmid DNA was isolated by miniprep as in [***2.5***]. DNA was sent to GATC Biotech AG for confirmation of the desired mutation by sequencing.

## 2.3. Molecular cloning by LIC

### 2.3.1. Primer design

Primers for Ligation Independent Cloning (LIC) into pET-YSBLIC3C were designed using the HiTel Primer Design Service, University of York Bioscience Technology Facility.

Primers were designed to have two parts; a pET-YSBLIC3C-complementary end and an insert-complementary end. The first 13 nucleotides from the 5' end of the forward primer (5'-CCAGGGACCAGCA-3'), and the first 17 nucleotides from the 5' end of the reverse primer (5'-GAGGAGAAGGCGCGTTA-3') were LIC3C-complementary. The remainder of the primer was insert-complementary. The reverse primer also adds a stop codon (TAA) to the gene of interest. This method allows addition of LIC3C-specific overhangs to the insertion gene by amplification.[83]

### 2.3.2. PCR using KOD Hot Start DNA polymerase

KOD Hot Start DNA polymerase (Merck Millipore) was used for molecular cloning due to its fidelity, speed, and proofreading ability. A PCR reaction mixture of 50 µL was assembled as described in ***Table 2.7***.

**Table 2.7** KOD Hot Start PCR reaction mixture.

| Component | Stock Concentration | Volume / µL |
|---|---|---|
| Autoclaved UPW | | 33 |
| KOD Hot Start buffer | 10x | 5 |
| dNTPs | 2 mM each nucleotide | 5 |
| DNA template (plasmid) | | 1 |
| Forward primer | 20 pmol $\mu L^{-1}$ | 1 |
| Reverse primer | 20 pmol $\mu L^{-1}$ | 1 |
| KOD Hot Start DNA polymerase | 1.0 U $\mu L^{-1}$ | 1 |

For standard PCR, thermocycling parameters were set as described in ***Table 2.8***.

**Table 2.8** KOD Hot Start standard PCR thermocycling parameters.

| Segment | Cycles | Temperature / °C | Time / s |
|---|---|---|---|
| Initialisation | 1 | 94 | 180 |
| Denaturation | 35 | 94 | 30 |
| Annealing | | 55 | 30 |
| Elongation | | 72 | 60 $kb^{-1}$ |
| Final elongation | 1 | 72 | 60 |
| Cooling | 1 | 4 | 120 |
| Hold | | 10 | ∞ |

For touchdown PCR, thermocycling parameters were set as described in ***Table 2.9***.

**Table 2.9** KOD Hot Start touchdown PCR thermocycling parameters.

| Segment | Cycles | Temperature / °C | Time / s |
|---|---|---|---|
| Initialisation | 1 | 95 | 180 |
| Denaturation | 15 | 95 | 60 |
| Annealing | | 70* | 30 |
| Elongation | | 72 | 60 $kb^{-1}$ |
| Denaturation | 20 | 95 | 60 |
| Annealing | | 55 | 30 |
| Elongation | | 72 | 60 $kb^{-1}$ |
| Final elongation | 1 | 72 | 90 |
| Cooling | 1 | 4 | 120 |
| Hold | | 10 | ∞ |

*decreases by 1 °C each cycle

### 2.3.3. Linearisation of pET-YSBLIC3C

To allow insertion of a gene into the vector pET-YSBLIC3C, the circular DNA must be linearised. This was accomplished by digesting the vector using the BseRI restriction enzyme through the reaction described in ***Table 2.10***.

**Table 2.10** pET-YSBLIC3C linearisation reaction mixture.

| Component | Volume / µL |
|---|---|
| Autoclaved UPW | 700 |
| Circular pET-YSBLIC3C | 180 |
| 10x CutSmart buffer (NEB) | 100 |
| BseRI | 20 |

Reaction was incubated at 37 °C for 110 min, then purified by agarose gel electrophoresis.

### 2.3.4. Agarose gel electrophoresis

Separation of DNA for analysis or purification was performed by agarose gel electrophoresis using a Bio-Rad Mini-Sub Cell GT electrophoresis system.

Agarose gel concentration was made to 1 % by dissolving 0.5 g agarose in 50 mL 1x TAE buffer by microwaving for 1 min, then addition of 1 µL SYBR Safe DNA gel stain before pouring. DNA was prepared by addition of 6x Purple Gel Loading Dye, and a 1 kb DNA ladder was loaded alongside samples.

Electrophoresis was run in 1x TAE buffer at 100 V for 60 min, and visualised under UV light for analysis or using an Invitrogen Safe Imager for band excision.

For DNA purification, the excised band of interest was purified using a GenElute Gel Extraction Kit (Sigma-Aldrich) according to the manufacturer's instructions. DNA was incubated for 30 min in 65 °C water then eluted.

### 2.3.5. T4 Polymerase treatment

Following PCR amplification of insertion gene with LIC3C-complementary overhangs and subsequent gel purification, both insert and vector DNA was treated with LIC-qualified T4 DNA polymerase (Novagen) to create sticky ends of the complementary regions. This was carried out as described in ***Table 2.11*** and ***Table 2.12***.

**Table 2.11** Gene insert T4 treatment reaction mixture.

| Component | Volume |
|---|---|
| 10x T4 DNA polymerase buffer | 2 µL |
| dATP (25 mM) | 2 µL |
| DTT (100 mM) | 2 µL |
| LIC-qualified T4 DNA polymerase | 0.4 µL |
| Insertion gene w/ overhangs | to final concentration of 0.2 pmol |
| Autoclaved UPW | to 20 µL |

**Table 2.12** Linear pET-YSBLIC3C T4 treatment reaction mixture.

| Component | Volume |
|---|---|
| 10x T4 DNA polymerase buffer | 6 µL |
| dTTP (25 mM) | 6 µL |
| DTT (100 mM) | 3 µL |
| LIC-qualified T4 DNA polymerase | 1.2 µL |
| Linear pET-YSBLIC3C | to final concentration of 0.6 pmol |
| Autoclaved UPW | to 60 µL |

Each reaction was incubated at 22 °C for 30 min, then 75 °C for 20 min. LIC3C reaction was purified by agarose gel electrophoresis.

### 2.3.6. Annealing

To anneal the insertion gene to pET-YSBLIC3C, both were incubated with each other at ratios of 1:1, 5:1, and 1:5 for 10 min at room temperature. This was followed by addition of 1 µL EDTA (25 mM) and incubation for a further 10 min at room temperature. Each reaction mixture was transformed into chemically competent *E. coli* as in [***2.4***].

### 2.3.7. Colony PCR

A master mix was assembled by multiplying ***Table 2.13*** by the total number of colonies required for testing, then dividing appropriately into 25 µL reactions.

**Table 2.13** Taq colony PCR reaction mixture master mix (1×).

| Component | Volume / µL |
|---|---|
| Autoclaved UPW | 18.6 |
| 10x standard *Taq* reaction buffer | 2.50 |
| dNTPs (2 mM each nucleotide) | 2.50 |
| $MgSO_4$ (50 mM) | 0.75 |
| Forward primer | 0.25 |
| Reverse primer | 0.25 |
| *Taq* DNA polymerase | 0.10 |

2 colonies were picked per plate, and each was touched to a division on an antibiotic agar plate (incubated at 37 °C), then rinsed in a 25 µL PCR reaction tube. Thermocycling parameters were as follows in .

**Table 2.14**.

**Table 2.14** Taq colony PCR thermocycling parameters.

| Segment | Cycles | Temperature / °C | Time / s |
|---|---|---|---|
| Initialisation | 1 | 95 | 30 |
| Denaturation | 30 | 95 | 30 |
| Annealing | | 55 | 60 |
| Elongation | | 68 | 60 $kb^{-1}$ |
| Final elongation | 1 | 68 | 300 |
| Cooling | 1 | 4 | 120 |
| Hold | | 10 | ∞ |

PCR was analysed by agarose gel electrophoresis, and successful colonies were picked from the division plate to inoculate starter cultures for miniprep to carry out a restriction digest.

### 2.3.8. Double restriction digest

Plasmids were analysed for successful cloning based on known patterns of fragmentation from digestion with restriction enzymes, using the following reaction as in ***Table 2.15***.

**Table 2.15** Double restriction digest reaction mixture.

| Component | Volume / µL |
|---|---|
| Plasmid DNA | 7 |
| 10x CutSmart buffer (NEB) | 1 |
| NcoI | 1 |
| NdeI | 1 |

Reaction was incubated at 37 °C for 180 min in a thermocycler. This was subsequently analysed by agarose gel electrophoresis.

## 2.4. Transformation into *E. coli* XL10-Gold for plasmid yield

Chemically competent *E. coli* XL10-Gold supplied by Agilent. Chemical competence by calcium chloride treatment increases membrane-DNA interactions.[84] A rapid change in temperature (heat shock) causes membrane pore formation allowing entry of proximal plasmid DNA.[85]

Transformation protocol followed manufacturer's instructions:

1) *E. coli* XL10-Gold competent cells thawed on ice and 50 μL mixed with 2 μL β-mercaptoethanol by gentle pipetting
2) Incubation on ice for 10 min with swirling
3) Addition of 1 μL plasmid DNA, gentle pipetting to mix
4) Incubation on ice for 30 min with swirling
5) Heat shock at 42 °C for 30 s in heat block
6) Incubation on ice for 2 min
7) Addition of 450 μL $NZY^+$ media warmed to 42 °C, gentle pipetting to mix
8) Incubation at 37 °C for 1 h while shaking at 200 RPM
9) 100 μL spread onto warm antibiotic agar plate (LB-kan); incubation at 37 °C overnight

## 2.5. Plasmid isolation by minipreparation

Plasmid DNA was isolated by miniprep, based on the alkaline lysis of cells and selective adsorption of plasmid DNA to a silica membrane. To prepare a starter culture, a 50 mL Falcon tube containing 5 mL autoclaved LB media with antibiotic (kanamycin at 50 μg $mL^{-1}$) was inoculated with a single colony of *E. coli* containing the plasmid of interest using a pipette tip. This was then placed in a shaker-incubator at 37 °C and 200 RPM overnight.

Cultures were harvested by centrifugation using a Sigma 3-16KL with rotor 1180 & 13190 at 3894 RCF. Plasmid isolation was carried out with a QIAprep Miniprep Kit (Qiagen) according to the manufacturer's instructions, eluting in 65 °C water. Centrifugation steps were carried out at 16,300 RCF using a Progen GenFuge 24D.

The DNA concentration was measured using the dsDNA function of an Eppendorf BioPhotometer plus.

## 2.6. Transformation into *E. coli* BL21(DE3) for expression

Chemically competent *E. coli* BL21(DE3) supplied by New England Biolabs (catalog number C2527H) were used as the heterologous expression host.

Transformation protocol followed manufacturer's instructions:

1) 50 µL tube of *E. coli* BL21(DE3) competent cells thawed on ice for 10 min
2) Addition of 1 µL plasmid DNA, gentle pipetting to mix
3) Incubation on ice for 30 min
4) Heat shock at 42 °C for 10 s in heat block
5) Incubation on ice for 5 min
6) Addition of 950 µL SOC media, gentle pipetting to mix
7) Incubation at 37 °C for 1 h while shaking at 200 RPM
8) 100 µL spread onto warm antibiotic agar plate (LB-kan); incubation at 37 °C overnight

## 2.7. Expression tests

Many factors affect the expression levels of recombinant genes, and thus the concentration and solubility of produced protein. These can include expression host, growth media, and induction temperature. An expression test allows analysis of gene expression while varying each of these factors, thus determining the ideal expression conditions.

A 5 mL starter culture of each transformant containing the enzyme plasmid in either *E. coli* BL21(DE3) or Rosetta(DE3) (Novagen) was made [***2.6***]. A 50 mL Falcon tube containing 10 mL of the test media with appropriate antibiotic(s) was prepared for each temperature and inoculated with 50 µL starter culture. For each tube, an identical control was prepared which would not be induced with IPTG.

All tubes were placed in a shaker-incubator at 37 °C and 200 RPM until an $OD_{600}$ of 1.7-2.0 (TB media) or 0.6-0.8 (M9 and LB media) was reached. Tubes other than the controls were induced with 1 mM IPTG (1M stock) and placed in a shaker-incubator set to the appropriate temperature and 180 RPM overnight.

Cultures were harvested by centrifugation using a Sigma 3-16KL with rotor 1180 & 13190 at 3894 RCF. Cell pellets were resuspended in 1 mL Buffer A and transferred to a 96-well block for sonication using a 24-tip multisample sonicator by repeating 90 cycles of 1 s sonication then 1 s cooling.

Soluble and insoluble fractions were separated by centrifugation using a Sigma 2K15 with rotor Nr.12148 at 15,000 RCF for 60 min at 4 °C. Each fraction was analysed by SDS-PAGE.

## 2.8. Gene expression

*E. coli* BL21(DE3) encodes an IPTG-inducible T7 RNA polymerase gene, which transcribes the gene of interest by binding to a T7 promoter site preceding the hexahistidine tag of pET-YSBLIC3C. IPTG is a lactose mimic which inactivates T7 repression at the lac operon, maintaining continuous T7 transcription as it is not metabolised. This allows overexpression of the gene of interest to produce protein at levels substantially higher than would normally be possible.

To uniformly inoculate multiple media, a starter culture of transformant *E. coli* BL21(DE3) containing the enzyme plasmid was made. Two 50 mL Falcon tubes containing 10 mL autoclaved LB media with antibiotic (kanamycin at 50 μg $mL^{-1}$) was inoculated with a single colony from [***2.6***], then placed in a shaker-incubator at 37 °C and 200 RPM overnight.

Ultra-Yield flasks (2.5 L) were prepared with 1 L TB media each and autoclaved [***2.1.4***]. Under sterile conditions, 100 mL Phosphate Salts, 1 mL kanamycin (1:1000, 50 mg $mL^{-1}$ stock) and 2 mL prepared starter culture from a single tube was added to each flask, then placed in a shaker-incubator at 37 °C and 300 RPM.

Upon reaching an $OD_{600}$ of 1.7-2.0 (TB media) or 0.6-0.8 (M9 and LB media), 1 mM IPTG (1M stock) was added for induction and flasks placed in a shaker-incubator at 16 °C and 250 RPM overnight.

## 2.9. Cell lysis

Flasks retrieved from shaker-incubator and contents centrifuged using a Beckman Coulter Avanti J-HC with a JLA-8.1000 rotor at 5000 RCF for 25 min at 4 °C.

Cell pellets may be transferred to 50 mL Falcon tubes and frozen in liquid nitrogen. For continuation, cell pellets were resuspended in 2 mL $g^{-1}$ Buffer A, then stirred at 4 °C to ensure homogeneity.

Cell lysis was performed by physical disruption, either through sonication or pressure. In the case of the former, the cell suspension was sonicated on ice using a MSE Soniprep 150 Plus by repeating 15 cycles of 30 s sonication then 45 s cooling with frequent swirling.

For the latter, a Constant Systems Ltd. Cell Disruptor was rinsed with water at 5 kpsi before loading cell suspension for lysis at 25 kpsi. This was followed by a rinse with Buffer A and lysate collection. System was cleaned at 5 kpsi with water then Triton detergent, and left in 20 % ethanol.

Lysate clarified by centrifugation using a Sorvall Evolution RC with a SS34 rotor at 50,000 RCF for 60 min at 4 °C. Supernatant filtered and loaded at 40 mL $h^{-1}$ onto a HisTrap FF Crude (5 mL) column (GE Healthcare) equilibrated with Buffer A, using a Peristaltic Pump P-1 (GE Healthcare).

## 2.10. Protein purification

### 2.10.1. Immobilized metal affinity chromatography (IMAC)

The six histidine residues incorporated onto the enzyme N-terminus by pET-YSBLIC3C form coordination bonds with nickel ($Ni^{2+}$) immobilised to the agarose-derived sepharose in the column. This retains the protein of interest in the column, allowing other undesired

proteins and soluble cellular substances to pass through. At this stage, an imidazole gradient is applied with a chromatography system and fractions are collected. Imidazole has competitive affinity for nickel, displacing histidine and freeing the protein into the buffer solution. Hexahistidine-tagged proteins will elute at a specific concentration of imidazole in the gradient, which is measured by UV as a chromatogram.

An ÄKTA chromatography system (GE Healthcare) was pump washed through lines B (Buffer C) then A (Buffer B). The protein-loaded HisTrap FF Crude column was connected and an affinity chromatography programme run. The programme consisted of the steps summarised in ***Table 2.16***.

**Table 2.16** IMAC purification programme for HisTrap FF Crude columns using ÄKTA systems.

| Step | Liquid composition as % of Line B | Volume passed / mL |
|---|---|---|
| Wash | 0 | 25 |
| Low Imidazole Wash | 4 | 25 |
| Gradient Elution | 4 - 100 | 100 |
| Final Elution | 100 | 25 |

The flow rate was set to 2.5 mL $min^{-1}$, and elute was collected as 1.8 mL fractions. These were subsequently analysed by SDS-PAGE.

### 2.10.2. Size exclusion chromatography (SEC)

Size exclusion chromatography relies on the separation of proteins based on their size, accomplished through the use of beads with a range of pore sizes. Small proteins can pass through more of these sizes than large proteins; thus the smaller the protein the more slowly it traverses the column, and the later it is eluted. For crystallography, this technique is used as a 'polishing' step and is particularly suitable for separating protein oligomers.

An ÄKTA chromatography system (GE Healthcare) was pump washed through lines B (Buffer B) then A (UPW, filtered and degassed). A HiLoad 16/600 Superdex 75 pg or 200 pg column (Ge Healthcare) was connected and an equilibration programme run as summarised in ***Table 2.17***. The flow rate was set to 1.0 mL $min^{-1}$.

**Table 2.17** Equilibration programme for HiLoad 16/600 Superdex columns using ÄKTA systems.

| Step | Liquid composition as % of Line B | Volume passed / mL |
|---|---|---|
| Wash | 0 | 120 (1.0 CV) |
| Equilibration | 100 | 132 (1.1 CV) |

Selected fractions collected from IMAC and analysed by SDS-PAGE were pooled and concentrated to < 2 mL in a Vivaspin 20 30k MWCO (Sartorius), using a Sigma 3-16KL centrifuge with a 1180 & 13190 rotor at 3894 RCF and 4 °C.

Concentrated protein was injected onto the ÄKTA system with a 2 mL loop and a SEC programme run. The programme consisted of the steps summarised in ***Table 2.18***.

**Table 2.18** SEC purification programme for HiLoad 16/600 Superdex columns using ÄKTA systems.

| Step | Liquid composition as % of Line B | Volume passed / mL |
|---|---|---|
| Wash | 100 | 20 |
| Elution | 100 | 100 |

The flow rate was set to 1.0 mL $min^{-1}$, and elute was collected as 1.8 mL fractions. These were subsequently analysed by SDS-PAGE.

Selected fractions were pooled and concentrated to 4 mg $mL^{-1}$ for flash-freezing and storage at -80 °C, or the appropriate concentration for crystallisation trials.

## 2.11. SDS-PAGE

Sodium dodecyl sulfate denatures proteins, allowing them to be analysed by secondary structure against molecular markers. The polyacrylamide gel restricts electric field-induced migration based on molecular mass (kDa).

SDS-PAGE gels were prepared at an acrylamide concentration of 12 %, as described in ***Table 2.19*** and ***Table 2.20***. Butan-1-ol was used to maintain a level surface during resolving gel polymerisation, before layering with the stacking gel and comb.

**Table 2.19** SDS-PAGE resolving gel (2×).

| Component | Volume |
|---|---|
| Autoclaved UPW | 3.2 mL |
| SDS-PAGE Resolving Buffer | 2.5 mL |
| Acrylamide | 4.2 mL |
| 10 % APS | 50 µL |
| TEMED | 8 µL |

**Table 2.20** SDS-PAGE stacking gel (2×).

| Component | Volume |
|---|---|
| Autoclaved UPW | 3.2 mL |
| SDS-PAGE Stacking Buffer | 1.3 mL |
| Acrylamide | 0.5 mL |
| 0.1 % bromophenol blue | 10 µL |
| 10 % APS | 25 µL |
| TEMED | 8 µL |

Protein samples were prepared by addition of 2x SDS-PAGE Sample Loading Buffer, then heated at 95 °C for 5 min. A low $M_w$ ladder was loaded alongside samples.

SDS-PAGE was run in SDS-PAGE Running Buffer at 200 V for 50 min, and stained with Coomassie.

## 2.12. Protein crystallisation

The vapour diffusion crystallisation method utilised in this work relies on the formation of vapour equilibration between the crystallisation condition reservoir and a drop of protein mixed with crystallisation condition. Vapour diffuses from the drop to the reservoir in a closed system, increasing the protein concentration to supersaturation for arrangement into crystals. This can either be performed by sitting drop or hanging drop method.

### 2.12.1. Sitting drop vapour diffusion

Sitting drop vapour diffusion crystallisation was carried out in 96-well format for condition screening.

A Hydra 96 (Robbins Scientific) was used to dispense 54 μL of each crystallisation condition into a 96-well MRC Wilden plate. A Mosquito LCP (TTP Labtech) mixed 150 nL SEC-purified protein with 150 nL crystallisation condition from the reservoir.

### 2.12.2. Hanging drop vapour diffusion

Wells of a 24-well cell culture plate (Cellstar) were filled with the constituent reagents of individual crystallisation conditions as defined by the manufacturer, with appropriate adjustment for optimisation. SEC-purified concentrated protein was mixed with well crystallisation condition on a siliconized glass coverslip, which was subsequently inverted and secured over the well with high vacuum grease (Dow Corning).

## 2.13. X-ray crystallography

The ordered arrangement of crystals can uniformly diffract an incidence beam of X-ray radiation, providing a diffraction pattern. This is subjected to Fourier transformation for conversion into a map of the protein's electron density, which is used as an 'outline' for secondary sequence orientation into a three-dimensional structure. Synchrotron light provides high-intensity radiation for collection of high-resolution electron density. Phases are refined using homologous proteins as molecular models.

Crystals were transferred into a cryoprotectant solution of the mother liquor containing 15% ethylene glycol and 5 mM linalool before flash-cooling with liquid nitrogen. A full dataset for LDIase C171S mutant was collected on beamline I02 at the Diamond Light Source, Didcot, Oxfordshire, U.K. Data were processed and integrated using XDS[86] and scaled using SCALA[87] within the Xia2[88] processing system. Data collection statistics can be found in ***Table 4.2*** (in [***Chapter 4***]). The structures were solved with MOLREP[89] using

one subunit of the structure of native LDIase (determined in the Grogan group) as the molecular replacement model. The structure was refined using iterative cycles of the programmes COOT[90] and REFMAC.[91]

## 2.14. LC-MS/MS

LC-MS/MS was performed by Dr Adam Dowle at the University of York Biosciences Technology Facility.

Samples separated by SDS-PAGE were excised, then destained and digested with Asp-N. LC-MS/MS analysis was performed over a 20 min gradient of elution.

# Chapter 3.

## *C. defragrans* Linalool Dehydratase-Isomerase (LDIase)

### 3.1. Expression and purification

A geraniol-bound complex of LDIase has previously been solved in the Grogan group through the use of a selenomethionine-substituted protein to overcome the phase problem. To develop a deeper understanding of the active site ligand-binding residues and possibly demonstrate a covalent intermediate, this project's initial objective was to use co-crystallisation methods to solve a linalool-bound complex.

The gene for the native enzyme Linalool Dehydratase-Isomerase from *Castellaniella defragrans* was cloned earlier into the pET-YSBLIC3C plasmid by S. Chambers. For the present work, a glycerol stock of bacteria containing this plasmid was used to isolate the DNA by miniprep with a yield of 130 ng $\mu L^{-1}$ [***2.5***].

Isolated plasmid was transformed into *E. coli* BL21(DE3) [***2.6***] and expressed in 3 L TB media [***2.8***]. Following a former successful method, cells were lysed by pressure homogenisation before nickel-based immobilised metal ion affinity chromatography (IMAC) (***Figure 3.1*** and ***Figure 3.2***). Although the UV absorbance indicated a high volume of eluted protein during IMAC purification on an ÄKTA start [***2.10.1***], the protein experienced high levels of precipitation upon concentration which made it unsuitable for size exclusion chromatography (SEC).

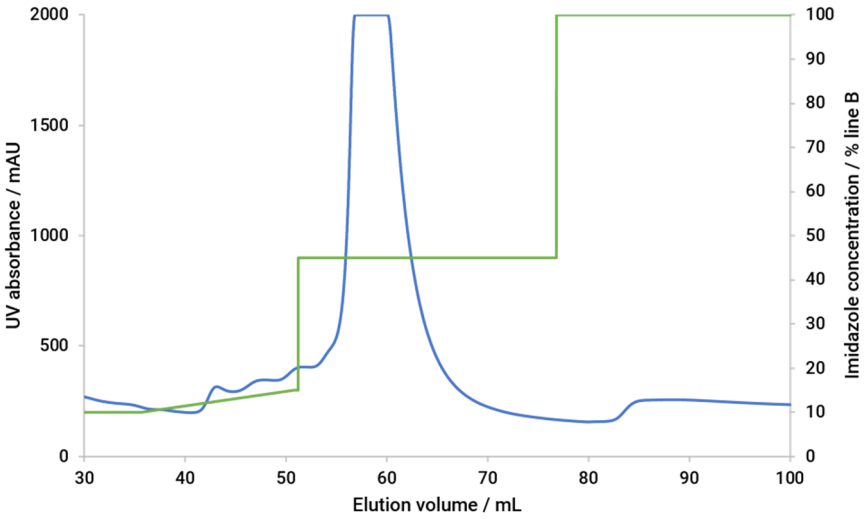


**Figure 3.1** Chromatogram of IMAC-purified native LDIase using an ÄKTA start, expressed in 3 L TB media and lysed by pressure homogenisation. The UV absorbance is shown in blue, with the imidazole gradient in green.

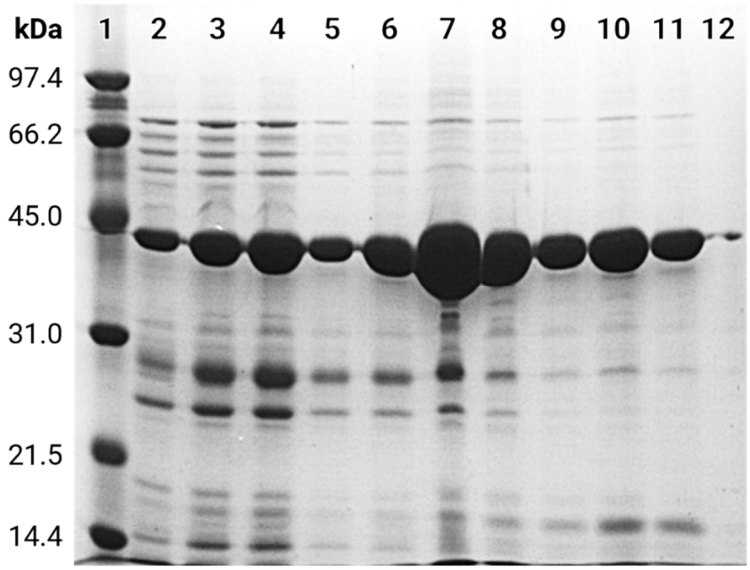


**Figure 3.2** SDS-PAGE of selected LDIase fractions from IMAC purification. Lane (1): low molecular weight marker; lanes (2-12): 5 mL fractions eluted by increasing imidazole concentration.

To prevent this precipitation, the purification procedure was repeated using sonicated rather than pressure homogenised cells, from 1 L TB expression rather than 3 L. Unfortunately, this provided a substantially reduced protein yield by IMAC (***Figure 3.3*** and ***Figure 3.4***).

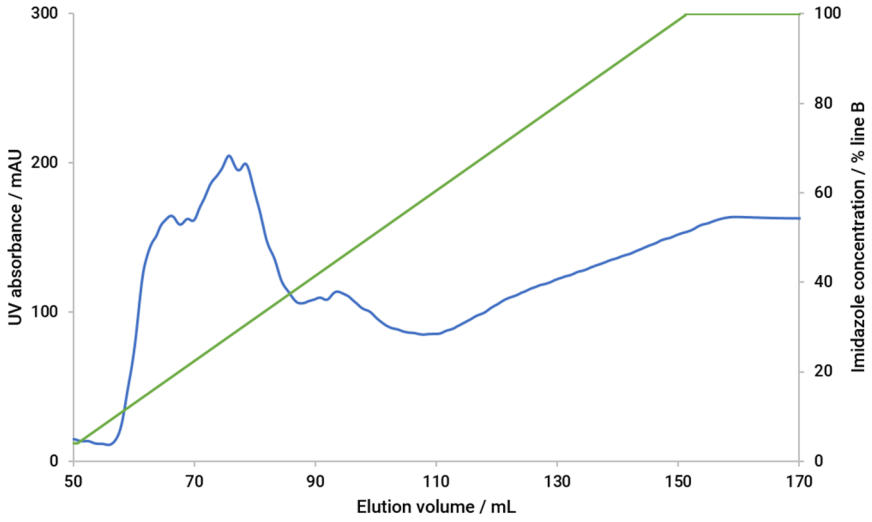


**Figure 3.3** Chromatogram of IMAC-purified LDIase using an ÄKTA start, expressed in 1 L TB media and lysed by sonication. The UV absorbance is shown in blue, with the imidazole gradient in green.

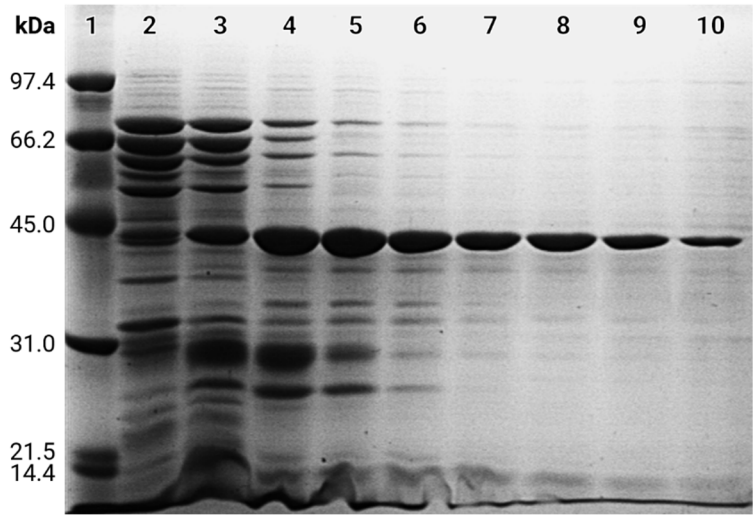


**Figure 3.4** SDS-PAGE of selected LDIase fractions from IMAC purification. Lane (1): low molecular weight marker; lanes (2-10): 5 mL fractions eluted by increasing imidazole concentration.

Nonetheless, fractions eluted between 85-105 mL were pooled and concentrated for SEC on an ÄKTA start the same day to prevent possible protein degradation [***2.10.2***] (***Figure 3.5*** and ***Figure 3.6***).

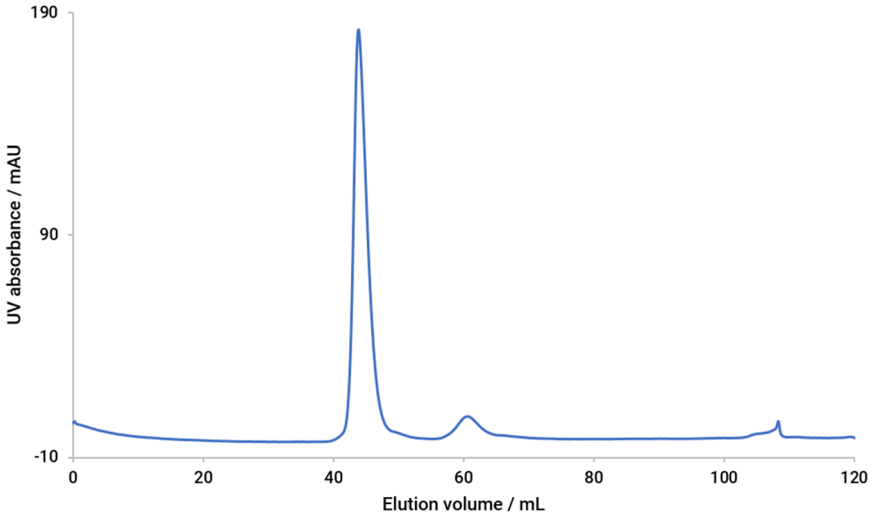


**Figure 3.5** Chromatogram of SEC-purified LDIase using a HiLoad 16/600 Superdex 75 pg column attached to an ÄKTA start.

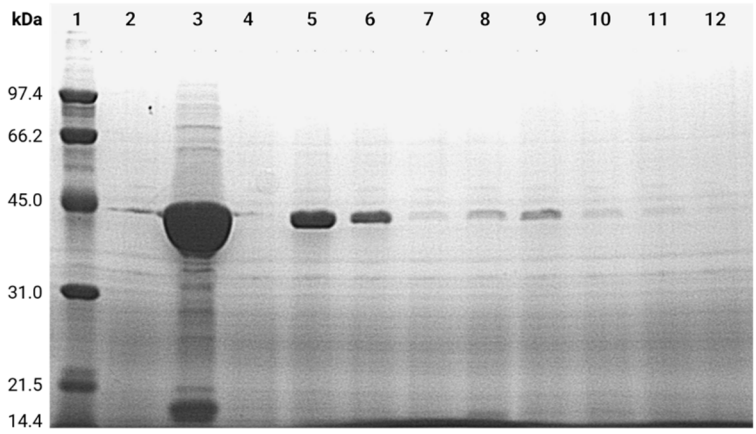


**Figure 3.6** SDS-PAGE of selected LDIase fractions from SEC purification. Lane (1): low molecular weight marker; lane (2): filtered clarified cell lysate; lane (3): pooled IMAC-purified protein; lanes (4-12): 5 mL fractions eluted by increasing imidazole concentration.

Although SEC fractions eluted between 40-45 mL were pooled, concentrated to 10 mg $mL^{-1}$ and flash frozen in liquid nitrogen for storage at -80 °C, the yield was too low for crystallisation trials. As such, protein previously purified by A. Hau & H. Man was used for co-crystallisation experiments with linalool.

## 3.2. Sitting drop crystallisation trials

Native LDIase purified by A. Hau & H. Man was concentrated to 10 mg $mL^{-1}$ and used to set up 96-well MRC Wilden plates for PACT, Index, and CSS I & II (with MES pH 6.0 and Tris

pH 8.0) [***2.12.1***]. For co-crystallisation with linalool, a 250 mM linalool stock in ethanol was used to give each mother liquor a linalool concentration of 0.5 mM.

After three days' incubation, crystal hits were observed across all three screens as noted in ***Table 3.1*** and ***Figure 3.7***.

**Table 3.1** Sitting drop crystallisation screens showing successful hit conditions.

| Crystallisation screen | Hit conditions | Chemical composition |
|---|---|---|
| CSS (+ 0.1 M MES pH 6.0) | D1 (CSS I) | 0.3 M Sodium acetate; 8 % PEG 20,000; 8 % PEG 550 MME |
| | F6 (CSS II) | 0.2 M Calcium acetate; 8 % PEG 20,000; 8 % PEG 550 MME |
| Index | B6 | 1.4 M (4.0 M $NaH_2PO_4$ + 4.0 M $K_2HPO_4$); pH 6.9 |
| | E11 | 0.02 M Magnesium chloride; 0.1 M HEPES; 22 % w/v Poly(sodium acrylate) 5100; pH 7.5 |
| PACT | F10 | 0.02 M (4.0 M $Na_2HPO_4$ + 4.0 M $KH_2PO_4$); 0.1 M Bis-Tris propane; 20 % w/v PEG 3350; pH 6.5 |
| | H12 | 0.2 M Sodium malonate dibasic monohydrate; 0.1 M Bis-Tris propane; 20 % w/v PEG 3350; pH 8.5 |

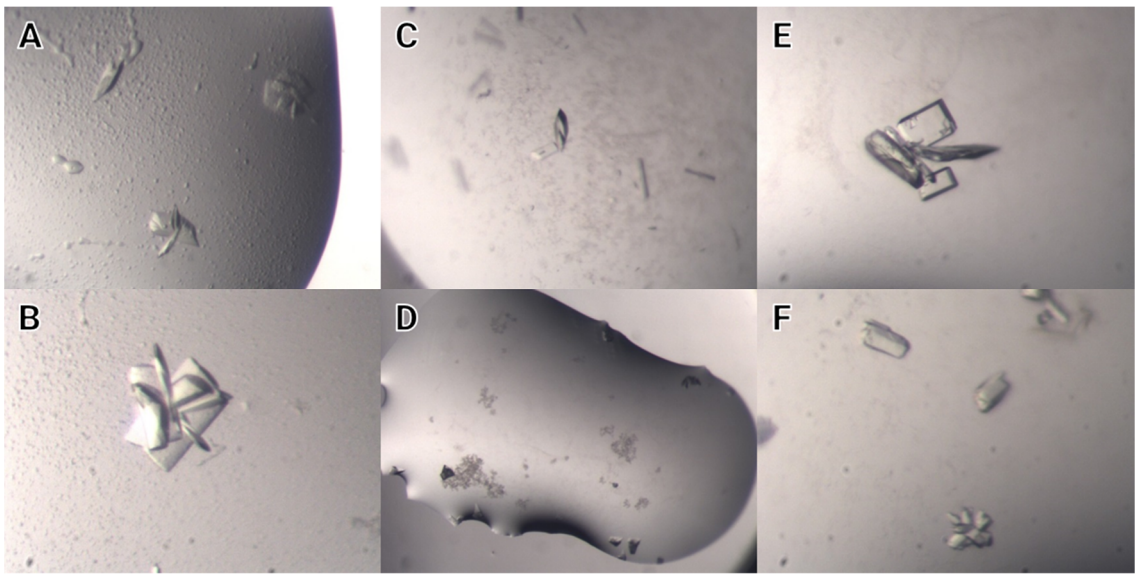


**Figure 3.7** Crystals from sitting drop screens of *C. defragrans* LDIase. (A): CSS D1; (B): CSS F6; (C): Index B6; (D): Index E11; (E): PACT F10; (F): PACT H12.

## 3.3. Optimisation trials for native LDIase purification

To produce LDIase for hanging drop vapour diffusion crystallisation scale-up trials, further attempts were made at purification for high yield and sufficient purity for crystal formation.

Cell pellets from 2 L TB expression that had been flash frozen were lysed by pressure homogenisation and purified by IMAC on an ÄKTA explorer (***Figure 3.8***).

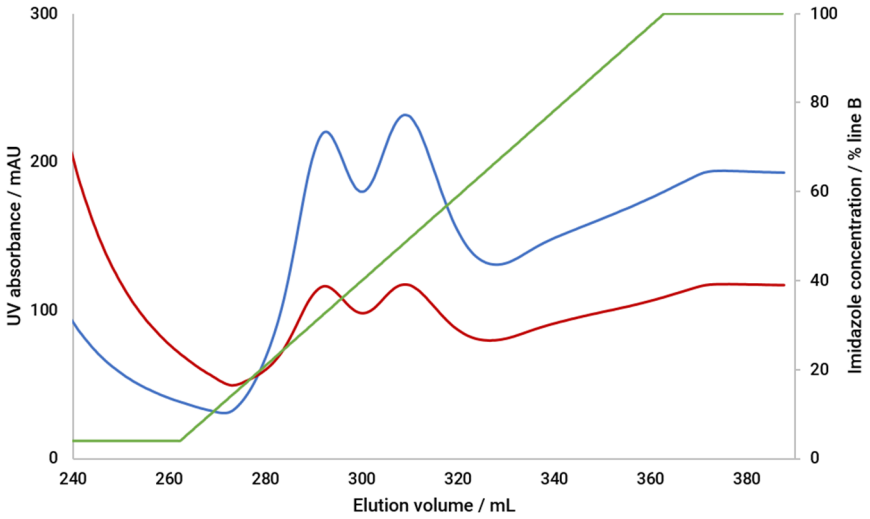


**Figure 3.8** Chromatogram of IMAC-purified LDIase using an ÄKTA explorer, expressed in 2 L TB media and lysed by pressure homogenisation. The $UV_{280nm}$ absorbance is shown in blue, $UV_{254nm}$ in red, and the imidazole gradient in green.

Fractions eluted between 295-323 mL were pooled and concentrated for SEC on the same system (***Figure 3.9***).

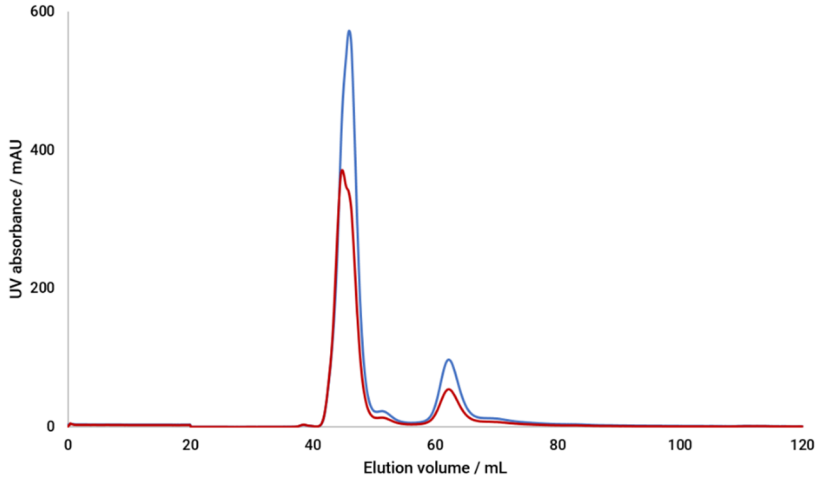


**Figure 3.9** Chromatogram of SEC-purified LDIase using a HiLoad 16/600 Superdex 75 pg column attached to an ÄKTA explorer. The $UV_{280nm}$ absorbance is shown in blue, and the $UV_{260nm}$ absorbance in red.

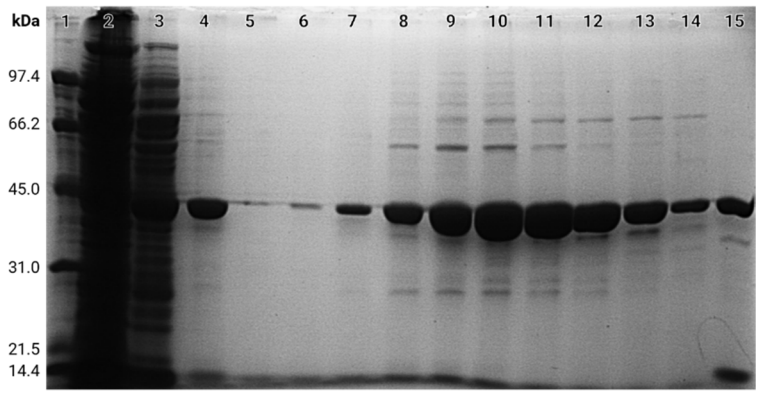


**Figure 3.10** SDS-PAGE of selected LDIase fractions from SEC purification. Lane (1): low molecular weight marker; lane (2): HisTrap FF Crude column loading flow-through; lane (3): IMAC-purification wash; lane (4): pooled IMAC-purified protein; lanes (5-15): 1.8 mL buffer-eluted fractions.

Although the chromatogram and SDS-PAGE gel (***Figure 3.10***) indicated pure protein, crystallisation did not occur with most of the protein precipitating in droplets. Further experiments in native LDIase purification failed to achieve crystallisable protein.

## 3.4. Linalool hanging drop crystallisation

24-well hanging drop vapour diffusion crystallisation trays were made for the successful sitting drop trial conditions Index B6, PACT F10, PACT H12, CSS D1 and CSS F6. Index E11 could not be made as polyacrylic acid 5100 was not available. Protein was used at a concentration of 10 mg $mL^{-1}$ and 10 μL of a 50 mM stock of linalool solution in ethanol was

added to make a final linalool concentration of 0.5 mM in each well. Of these conditions, only PACT F10 yielded good quality crystals.

To test whether the ethanol present in the linalool stock affected crystal growth, the PACT F10 condition was repeated, however rather than adding the 50 mM linalool stock, 1.1 μL of source linalool was added to each well of the lower two rows. This appeared to show little difference in the resulting crystals.

An additive screen for the purpose of optimisation to develop larger crystals by slower growth was made. Ethylene glycol and glycerol were varied by 1-5 %, and ratios of 2:1 and 1:1 of protein to condition were trialled. Conditions with ethylene glycol and drops in a ratio of 2:1 grew the best crystals. This was carried out over all the original conditions used for hanging drop, however PACT F10 remained the most successful.

Additional optimisation adjusted PEG 3350 from 14-24 %; ethylene glycol from 2-6 %; and sodium/potassium phosphate from 14-24 mM. Protein to condition ratios were varied as above, using 2:1 and 1:1. Many large crystals resulted from these, specifically the 2:1 drops, however 14 % PEG 3350 and 24 mM sodium/potassium phosphate with 2% ethylene glycol yielded the best.

To test other protein to condition ratios, another optimisation in PACT F10 was set up using ratios of 1:1, 2:1, 1:2, and 3:1 respectively. However, this gave inconsistent results with sporadic differences in crystal quality.

Although some of the best crystals amongst the hanging drop optimisations generated good diffraction patterns and data was collected, a brief examination of the datasets did not show ligand density. Therefore, further PACT F10 24-well trays were made with the linalool concentration increased from 0.5 mM in each well to 5 mM, with variations in ethylene glycol of 4-6 % and PEG 3350 of 12-14 % (***Figure 3.11***). Even with this increase the substrate-complexed structure continued to remain elusive. Crystal soaking over a period of approximately four hours also did not yield such ligand density from collected datasets.

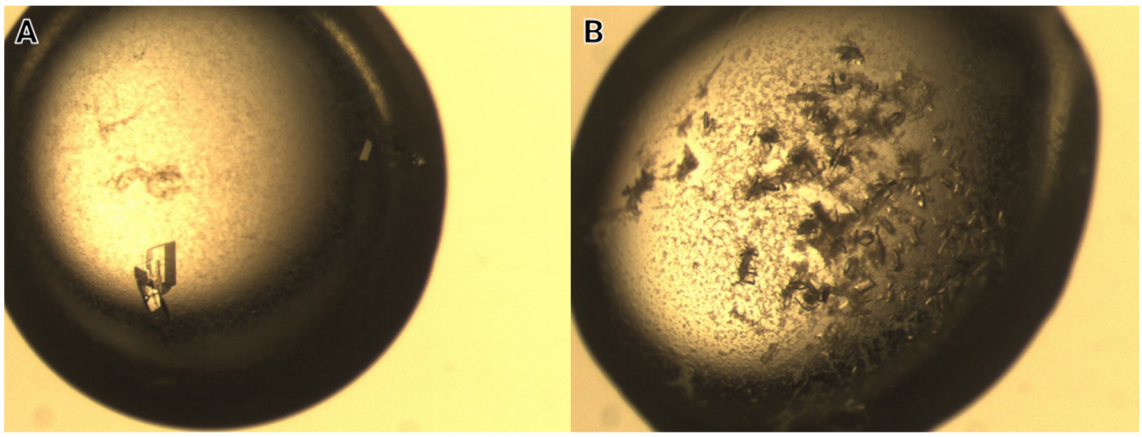


**Figure 3.11** Hanging drop crystals of LDIase in 5 mM linalool. (A): 14 % PEG & 4 % ethylene glycol; (B): 24 mM sodium/potassium phosphate & 2 % ethylene glycol.

## 3.5. Geraniol hanging drop crystallisation

It is reported by the literature that the equilibrium of the LDIase enzyme lies towards myrcene.[71] Therefore, a possible method for forming a linalool complex may be to co-crystallise the enzyme with geraniol rather than linalool to 'trap' it in a complex after substrate conversion.

Hanging drop trays were set up as for linalool, however using 5 mM geraniol in each well. PACT F10 was used, varying PEG 3350 from 12-14 % across one axis, and ethylene glycol from 4-6 % across the other. Crystal yield was high, with the best found in 14 % PEG 3350 with 6 % ethylene glycol. Soaking of these crystals with geraniol as above was also attempted. These crystals diffracted well and supplied datasets, however without ligand density.

## 3.6. LC-MS/MS

To supply further evidence of a covalent LDIase-linalool intermediate complex, LC-MS/MS analysis of SDS-PAGE separated samples was performed by Adam Dowle of the Bioscience Technology Facility [***2.14***] (***Figure 3.12***). If the suspected residues involved in intermediate formation Cys 171 or Cys 180 were covalently bound to linalool, a mass addition of 122.1 Da to one of these peptide residues should be observed over the untreated control. Unfortunately, no such mass addition was identified. Repeating this experiment with C171S or C171A 'slow' mutants may encourage retention of the prospective intermediate.

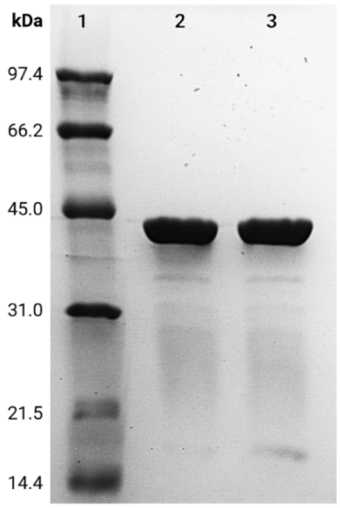


**Figure 3.12** SDS-PAGE of LDIase incubated in linalool for LC-MS/MS analysis.

## 3.7. Conclusions

Repeated attempts at co-crystallisation of native LDIase did not yield any ligand-bound complexes or any indication of such. As the protein used had previously produced a ligand-bound complex, this was unlikely to be the source of the issue. It is possible that the ethanol used to solubilise linalool for accurate concentration control during addition inactivated the enzyme. However, trays set up without ethanol by direct addition of linalool also failed to present a ligand-bound complex. This could indicate a problem with the compatibility with LDIase of the co-crystallisation method used, or could encourage optimisation of soaking length.

As an alternative method for determining the existence of a covalent intermediate and ligand-binding determinants, the investigation of the cysteine believed to form the covalent bond to the intermediate could be performed. Two mutants can be used for this; serine (C171S) and alanine (C171A) would both have steric similarities to C171 and allow for the creation of a 'slow' mutant to hold the predicted intermediate during X-ray diffraction.[81]

# Chapter 4.

## Linalool Dehydratase-Isomerase mutagenesis, C171S

### 4.1. Mutagenesis

Mutagenesis was carried out as a variation of the QuickChange method described in section [***2.2***] using touchdown PCR and SOC media without β-mercaptoethanol for transformation, however no colonies grew. The competency of XL-10 Gold cells was verified by a control transformation, which was successful. This indicated a problem with the PCR step. A series of optimisations were attempted in order to determine and overcome this limiting step, as summarised in ***Table 4.1***.

**Table 4.1** Rounds of LDIase C171S mutagenesis attempts using LDI_C171S_FOR and LDI_C171S_REV primers. Each attempt was followed the same protocol, but with the exceptions described.

| Attempt | Condition changed | Details |
|---|---|---|
| 1 | Initial mutagenesis | |
| 2 | Larger graduations for PCR temperature stepdown of touchdown cycle | 1 °C annealing temperature decrease for each cycle changed to 0.5 °C |
| 3 | Use of standard thermocycling conditions to replace touchdown | Annealing temperature for each cycle changed to 55 °C, for 30 cycles |
| 4 | Dilution of template DNA | 1 μL of 10 ng $\mu L^{-1}$ DNA added instead of 130 ng $\mu L^{-1}$ |
| 5 | Change in DNA polymerase | Pfu Turbo replaced with KOD Hot Start (replacing 1 μL $H_2O$ with 25 mM $MgSO_4$) |
| 6 | Addition of DMSO | 1 μL DMSO added to reaction for 2 % total concentration |

None of these changes yielded colonies after the transformation step. The issue was suspected to lie with the mutagenesis primers, and thus new primers were designed with a single base change and higher melting temperature.

Newly designed primers were used for mutagenesis [***2.2***]. Colonies successfully grew and DNA was isolated by miniprep [***2.5***].

## 4.2. Expression and purification

Isolated LDIase C171S mutant plasmid DNA was transformed into *E. coli* BL21(DE3) [***2.6***] and expressed in 2 L TB media [***2.8***]. Cells were lysed by sonication [***2.9***] and purified initially by IMAC [***2.10.1***] on an ÄKTA pure (***Figure 4.1***). SDS-PAGE analysis provided further information on the fractionation contents [***2.11***] (***Figure 4.2***).

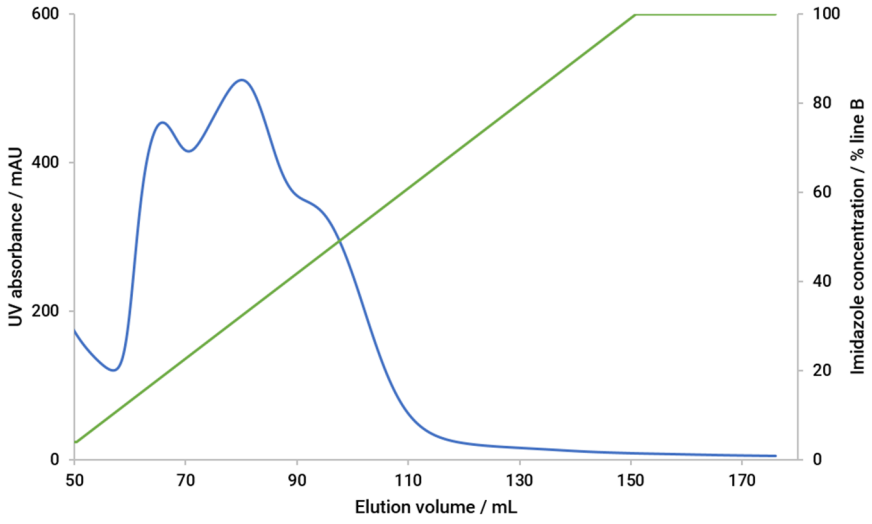


**Figure 4.1** Chromatogram of IMAC-purified LDIase mutant C171S using an ÄKTA pure, expressed in 2 L TB media and lysed by sonication. The UV absorbance is shown in blue, with the imidazole gradient in green.

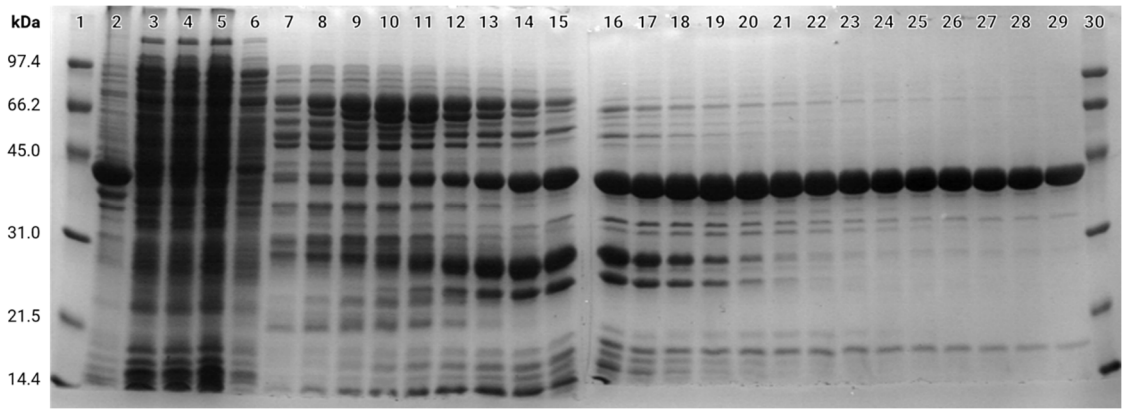


**Figure 4.2** SDS-PAGE of selected LDIase mutant C171S fractions from IMAC purification. Lanes (1 & 30): low molecular weight marker; lane (2): 1:10 dilution of the insoluble fraction; lane (3): 1:5 dilution of the unfiltered clarified cell lysate; lane (4): 1:5 dilution of the filtered clarified cell lysate; lane (5): HisTrap FF Crude column loading flow-through; lane (6): IMAC-purification wash; lanes (7-29): 1.8 mL fractions eluted by increasing imidazole concentration.

Interestingly, the IMAC chromatogram showed a visibly different peak to native LDIase chromatograms. Rather than a single peak or a doublet peak, a triplet peak is observed. This could be due to better purification, or a chromatographic difference from the mutation. SDS-PAGE analysis indicated the first peak of the triplet was not pure and contained many proteins of the incorrect size. The second peak was shown to contain the protein of interest with a smaller-sized impurity. The third and final sloped peak contained the pure protein of interest (fractions 2B9-2C12), which was pooled and concentrated for SEC using an S200 16/600 pg column on an ÄKTA pure [***2.10.2***] (***Figure 4.3***).

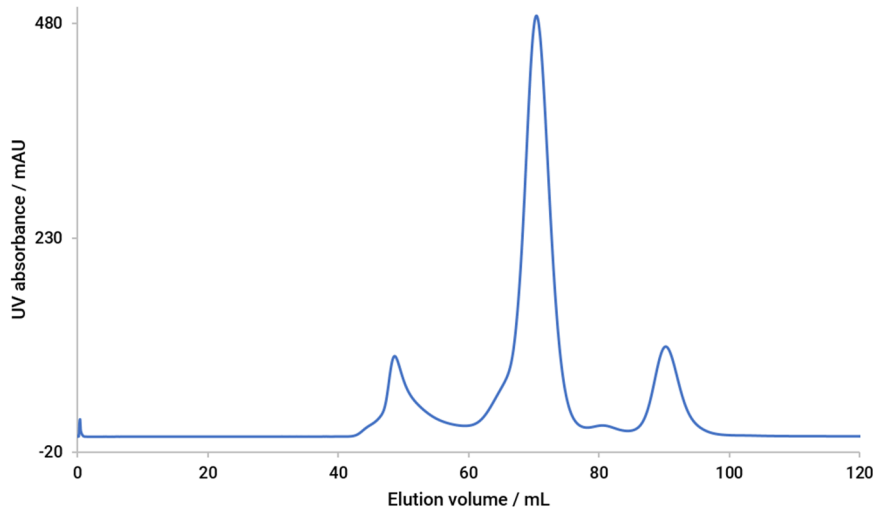


**Figure 4.3** Chromatogram of SEC-purified LDIase mutant C171S using a HiLoad 16/600 Superdex 200 pg column attached to an ÄKTA pure.

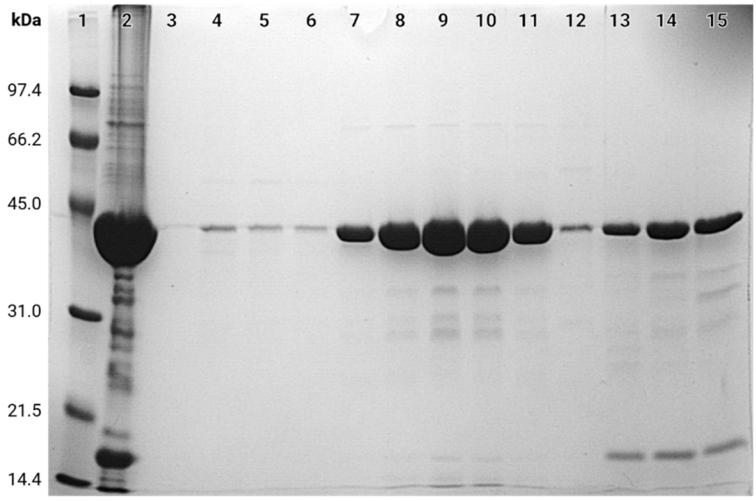


**Figure 4.4** SDS-PAGE of selected LDIase mutant C171S fractions from SEC purification. Lane (1): low molecular weight marker; lane (2): pooled IMAC-purified protein; lane (3): SEC-purification waste; lanes (4-15): 1.8 mL buffer-eluted fractions.

The SEC chromatogram also showed three peaks, compared to the two given by the native enzyme. SDS-PAGE analysis (***Figure 4.4***) showed that the second, tallest peak had the cleanest protein. This was also suspected to be the correct oligomeric conformation for crystallisation, however details of the oligomer could not be determined without running an Analytical SEC experiment. Fractions from this peak (2C1-2C4) were pooled and used for crystallisation trials.

## 4.3. Crystallisation

LDIase C171S protein was concentrated and used to set up 96-well MRC Wilden plates for PACT, Index, and CSS I & II (with MES pH 6.0 and Tris pH 8.0) [***2.12.1***]. The top well used a protein concentration of 12 mg $mL^{-1}$ and the bottom well 6 mg $mL^{-1}$.

Crystals were found in PACT F10, Index E11 and CSS D4 (MES pH 6.0), all at 12 mg $mL^{-1}$ (***Figure 4.5***).

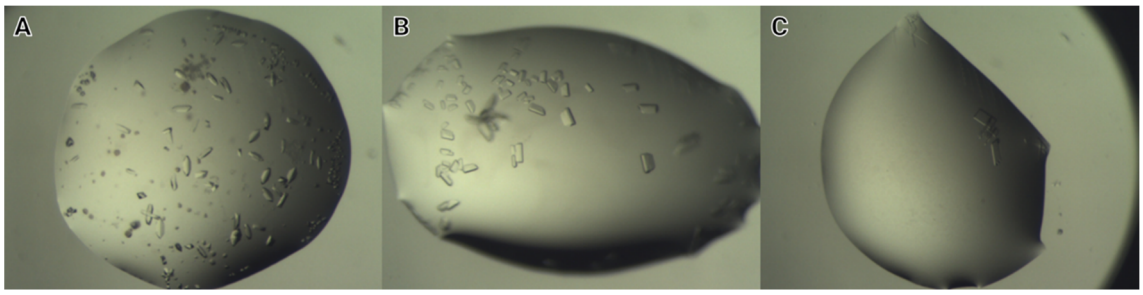


**Figure 4.5** Crystals from sitting drop screens of LDIase mutant C171S added at a concentration of 12 mg $mL^{-1}$. (A): PACT F10; (B): Index E11; (C): CSS D4 (+ MES pH 6.0).

PACT F10 and Index E11 provided the best crystals, and so were selected for expansion to 24-well hanging drop crystallisation. In hanging drop optimisation of both screens, all three condition components were adjusted. For PACT F10, PEG 3350 ranged from 16-22 %; bis-tris propane from 80-120 mM; and sodium/potassium phosphate from 10-30 mM. For Index E11, poly(acrylic acid sodium salt) 5,100 ranged from 18-24 %; HEPES 0.1 M from pH 7.0-8.0; and magnesium chloride hexahydrate from 10-30 mM.

To attempt to gain a substrate-bound complex of the mutant, the conditions above were repeated with co-crystallisation using a method different than that which had unsuccessfully been attempted for the native protein. For a linalool concentration of 10 mM, 0.13 μL linalool was added to 100 μL LDIase C171 protein at 8 mg $mL^{-1}$. This stock was then used in the preparation of hanging drop optimisation trays.[92]

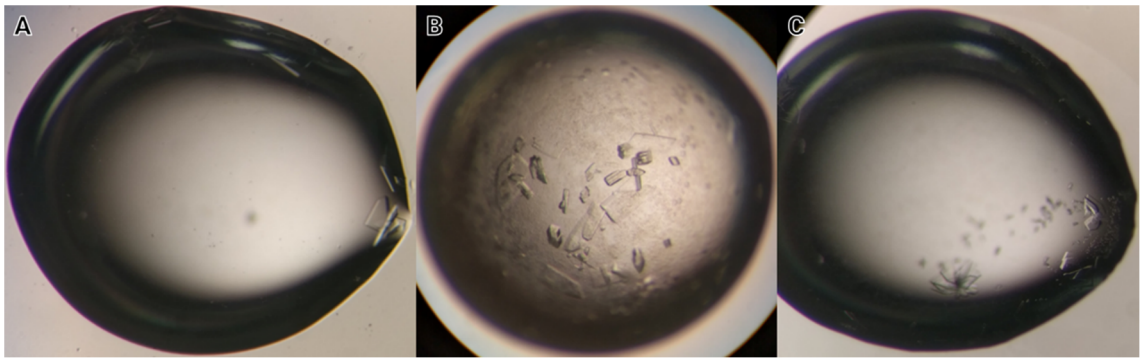


**Figure 4.6** Hanging drop crystals of LDIase mutant C171S. (A): PACT F10 C1 2:1 (protein:reservoir) 10 mg mL-1; (B): PACT F10 + 10 mM linalool 1:1 (protein:reservoir) B1; (C): PACT F10 + 10 mM linalool 1:1 (protein:reservoir) C1.

Drops producing high-quality crystals (***Figure 4.6***) were fished and tested, before being sent for data collection at Diamond Light Source.

## 4.4. X-ray crystallography

A crystal from PACT F10 B1 diffracted to 2.58 Å resolution, with associated data collection statistics described in ***Table 4.2***. A Matthews coefficient value of 2.56 was calculated, suggesting a maximal probability of ten molecules in the asymmetric unit and a 52 % solvent content.

**Table 4.2** Data collection and refinement statistics for LDIase mutant C171S. Numbers in brackets refer to data for the highest resolution shells.

| | **LDIase C171S** |
|---|---|
| Beamline | Diamond I02 |
| Wavelength (Å) | 0.9795 |
| Resolution (Å) | 76.52-2.58 (2.62-2.58) |
| Space Group | $P2_1$ |
| Unit cell (Å) | a = 87.77; b = 109.47; c = 232.70<br>α = γ = 90°; β = 99.5° |
| No. of molecules in the asymmetric unit | 10 |
| Unique reflections | 135904 (6447) |
| Completeness (%) | 99.3 (96.0) |
| $R_{merge}$ (%) | 0.11 (0.74) |
| $R_{p.i.m.}$ | 0.09 (0.64) |
| Multiplicity | 4.1 (3.7) |
| $<I/\sigma(I)>$ | 8.7 (1.7) |
| Overall *B* factor from Wilson plot (Å$^2$) | 39 |
| $R_{cryst}$/ $R_{free}$ (%) | 18.2/21.1 |
| r.m.s.d 1-2 bonds (Å) | 0.01 |
| r.m.s.d 1-3 angles (°) | 1.47 |
| Avge main chain B (Å$^2$) | 43 |
| Avge side chain B (Å$^2$) | 47 |
| Avge water B (Å$^2$) | 39 |

The monomer of native LDIase was used to solve the structure of the mutant C171S using MOLREP over ten copies of the search set [***2.13***]. Coincidentally, the asymmetric unit was found to contain ten molecules constituting two dimers (***Figure 4.7***), whereas previously solved LDIase structures constituted a single pentamer.

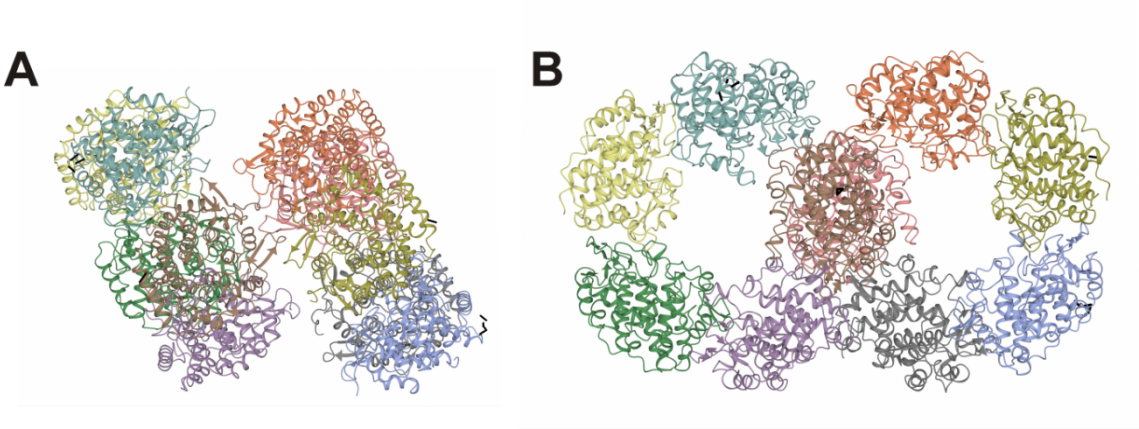


**Figure 4.7** The X-ray crystallographic structure of the LDIase mutant C171S, consisting of a ten-molecule asymmetric unit. (A): lateral view; (B): anterior view.

REFMAC and COOT were used for the initial refinement, followed by iterative rounds of building and further refinement [***2.13***]. Each active site at the monomer interface showed red negative difference density for the side chain of residue 171, showing an occupancy error for cysteine which was corrected when changed to serine, thus confirming the mutation.

The structure displayed conspicuous differences to side change positions of certain residues in the active site (***Figure 4.8***). As residue 171 no longer possessed the sulfur of cysteine, it could not form a disulfide bridge with Cys 180. Additionally, Trp 244 had reoriented to point away from the ligand binding site. It is possible that this is due to complexation with a ligand.

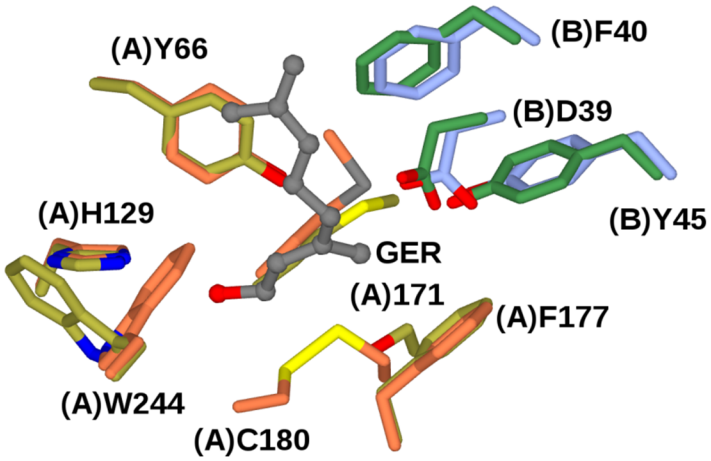


**Figure 4.8** The LDIase mutant C171S superimposed with the previously determined geraniol-bound structure. For the latter complex, the carbon atoms of subunits (A) and (B) are coloured coral and green respectively, with geraniol in grey. The carbon atoms of C171S subunits (A) and (B) are coloured gold and light blue respectively. The side chain of W244 is seen to move away from the ligand binding site in the C171S structure.

Additional density was observed in the active site extending from Cys 180 which did not match the enzyme's amino acid residues (***Figure 4.9***). Unfortunately, as for datasets of native LDIase, this occupancy could not be defined as ligand density corresponding to linalool, geraniol or myrcene. However, it could provide the first indication that Cys 180 acts as a nucleophile as proposed in the reaction mechanism, forming a covalent thioterpene intermediate.

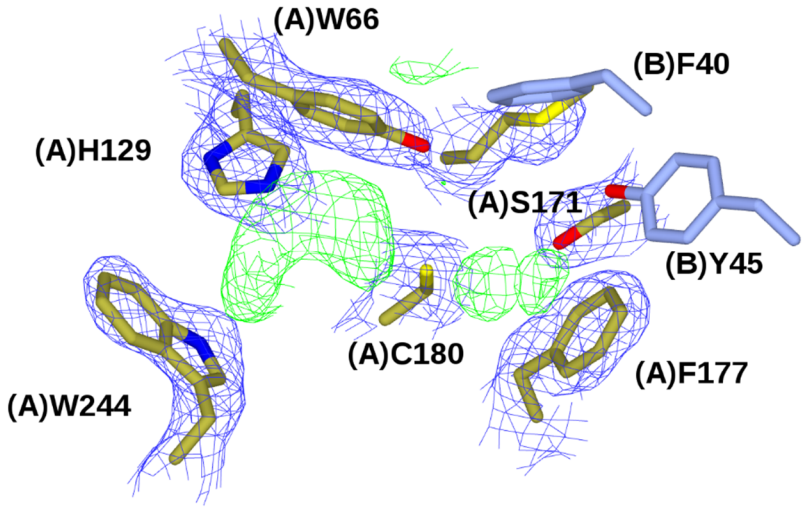


**Figure 4.9** The active site of the LDIase mutant C171S showing its electron density. The carbon atoms of subunits (A) and (B) are coloured gold and light blue respectively. The electron density corresponds to the Fo-Fc (omit) and 2Fo-Fc maps, which are shown in green and blue at levels of 3σ and 1σ respectively. Clear electron density can be observed extending from the side-chain of C180, possibly indicating the low occupancy of a covalent bond to a ligand.

# Chapter 5.

## *R. erythropolis* Linalool Dehydratase-Isomerase (ReLDIase)

### 5.1. Molecular cloning

To confer a hexahistidine tag to the N-terminus of ReLDIase, the synthesised gene required cloning into an appropriate vector, in this case pET-YSBLIC3C. This was accomplished by Ligation Independent Cloning (LIC) [***2.3***]. The gene of interest was amplified by PCR from the host pMK-RQ (kanR) plasmid as supplied by Invitrogen. The amplified gene was purified by gel extraction to give a yield of 121.7 ng $\mu L^{-1}$. This was then treated with T4 polymerase prior to annealing with linearised pET-YSBLIC3C vector (57 ng $\mu L^{-1}$). Three different ratios of gene insert to vector were trialled as optimisation in the annealing step; 1:1, 1:5, and 5:1. Each of these reactions was transformed into *E. coli* [***2.4***].

Colony PCR of each transformant carried out to provide an indication of success [***2.3.7***]. An agarose gel of these (***Figure 5.1***) suggested that all annealing reactions were successful, showing a band corresponding to the insert size of 1698 bp, however due to the possible amplification of unannealed background DNA insert this was not sufficient to confirm.

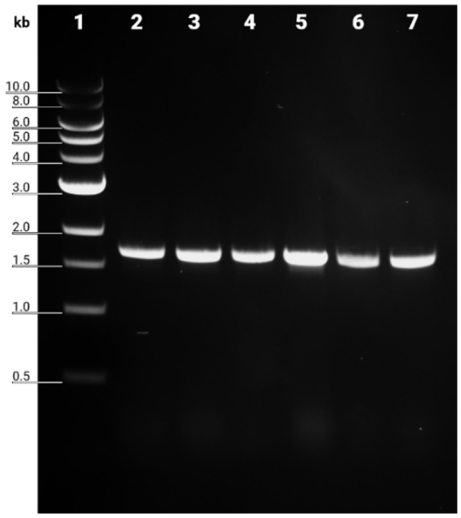


**Figure 5.1** An agarose gel of colony PCR to test the success of ReLDIase gene cloning into pET-YSBLIC3C. Bands are visible at 1.7 kb, matching the insert size.

A double restriction digest using NcoI and NdeI was carried out of two transformants from annealing reactions of ratios 1:5 and 3:3 [***2.3.8***]. The agarose gel (***Figure 5.2***) did not show all expected bands, missing 904 bp, 441 bp, 354 bp, and 86 bp. Fortunately, a band corresponding to the expected fragment size of 5308 bp was visible, which could suggest a successful cloning reaction.

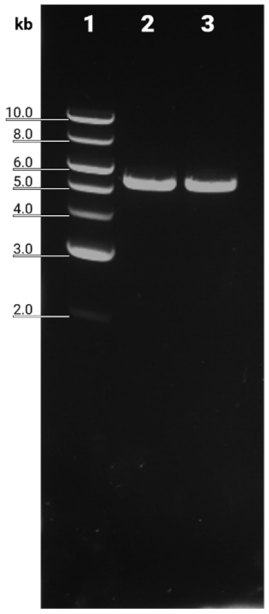


**Figure 5.2** A double restriction digest to test the success of ReLDIase gene cloning into pET-YSBLIC3C. The two visible bands match an expected fragment size of 5.3 kb.

Sequencing by GATC (T7 forward, pET-RP reverse) was used to confirm molecular cloning of gene into pET-YSBLIC3C. Results showed 99.7 % sequence identity due to an unresolved nucleotide encoding the codon for K276, though this is most likely a sequencing error. Thus, cloning was considered successful.

## 5.2. ReLDIase expression tests

Expression tests were carried out to investigate the effect of changing expression host, growth media, and induction temperature [***2.7***] (***Figure 5.3***, ***Figure 5.4***, and ***Figure 5.5***). Expression hosts tested were *E. coli* BL21(DE3) and *E. coli* Rosetta(DE3). Growth media tested were M9, LB, and TB. Induction temperatures tested were 16 °C, 25 °C (not including LB), 30 °C, and 37 °C.

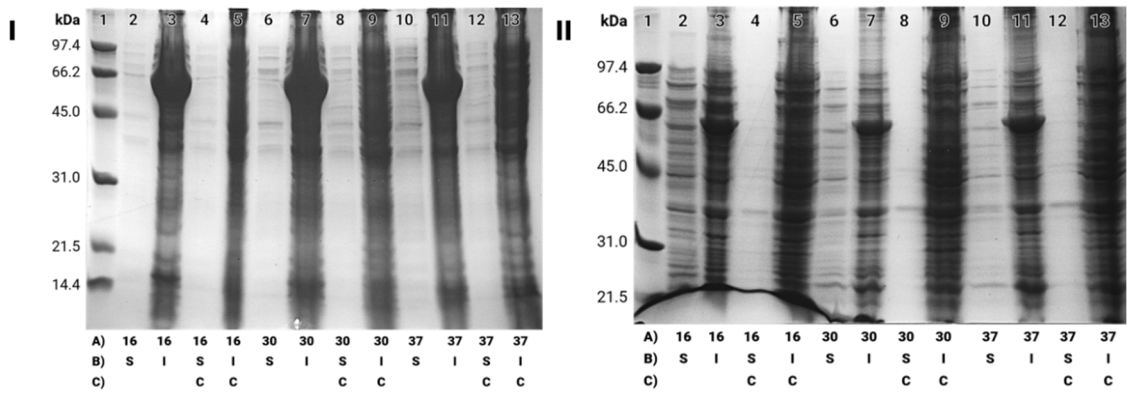


**Figure 5.3** ReLDIase expression tests in LB media. (I): BL21 expression host; (II): Rosetta expression host. A) denotes induction temperature; B) denotes soluble (S) or insoluble (I) fractions; C) denotes controls (C).

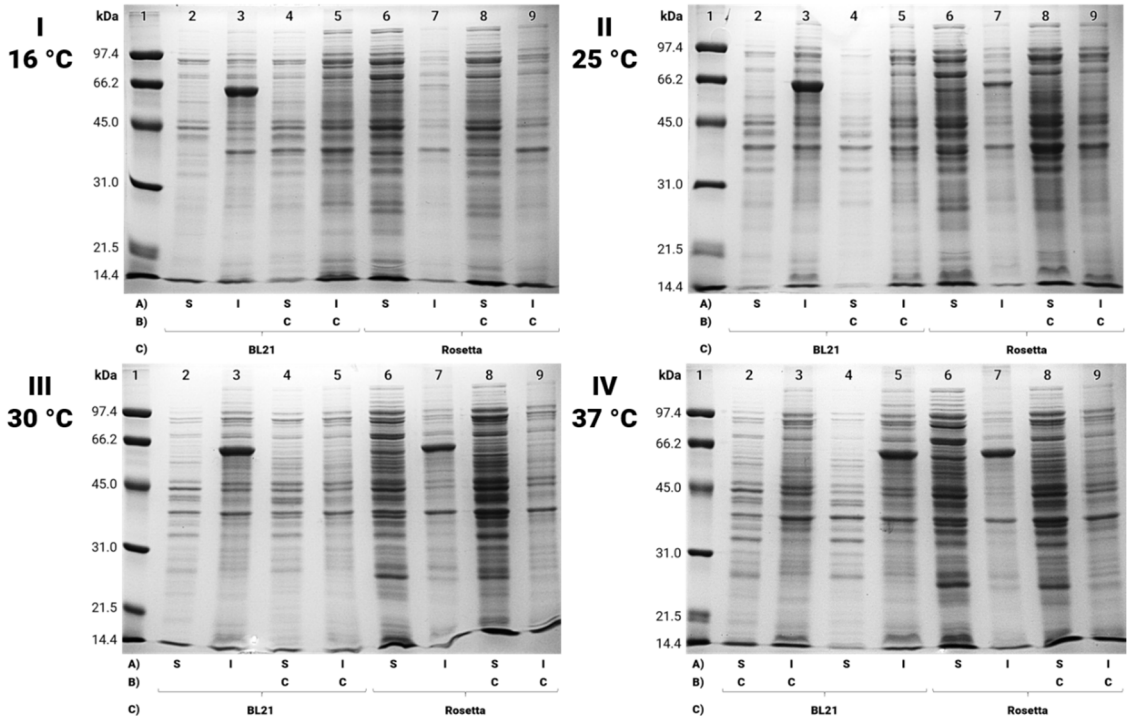


**Figure 5.4** ReLDIase expression tests in M9 media. Temperatures of induction are shown to the top right of each gel. A) denotes soluble (S) or insoluble (I) fractions; B) denotes controls (C); C) denotes expression host.

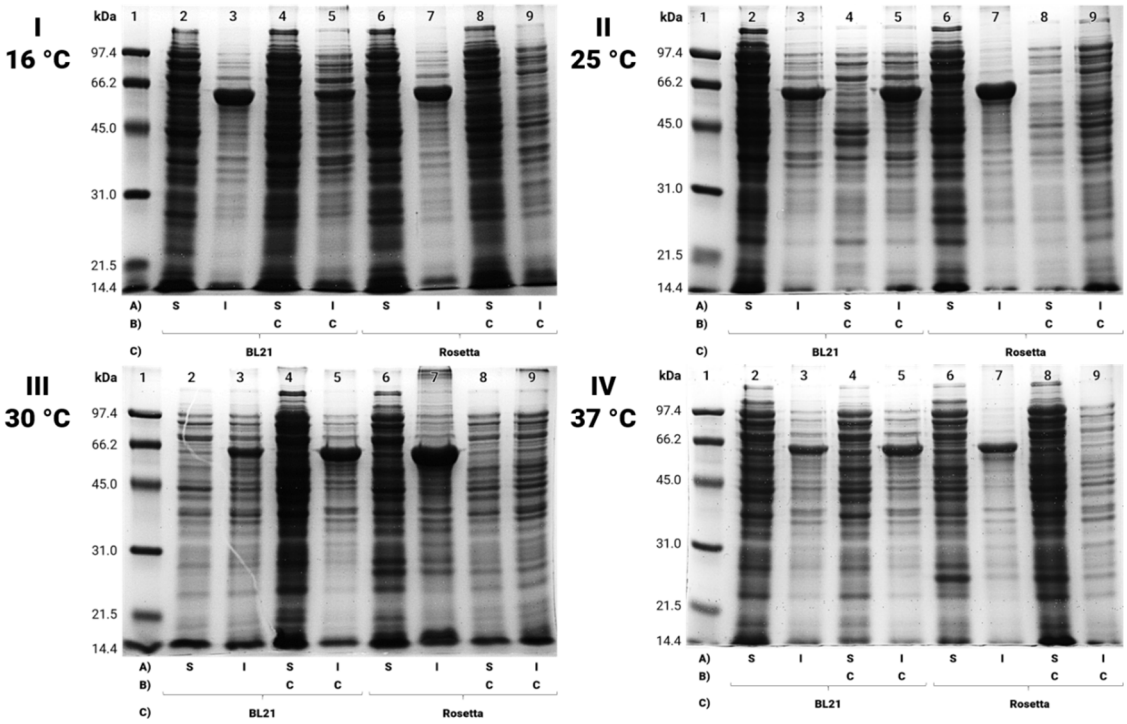


**Figure 5.5** ReLDIase expression tests in TB media. Temperatures of induction are shown to the top right of each gel. A) denotes soluble (S) or insoluble (I) fractions; B) denotes controls (C); C) denotes expression host.

Expression levels were high, though no protein solubility was observed to allow larger-scale expression for purification.

## 5.3. ReLDIase expression and purification

To test if sufficient ReLDIase may be made for purification at a larger scale of expression, 4 L LB media was inoculated with ReLDIase in *E. coli* BL21(DE3) before 16 °C induction then pressure homogenisation. IMAC purification was performed on an ÄKTA start [***2.10.1***] (***Figure 5.6***).

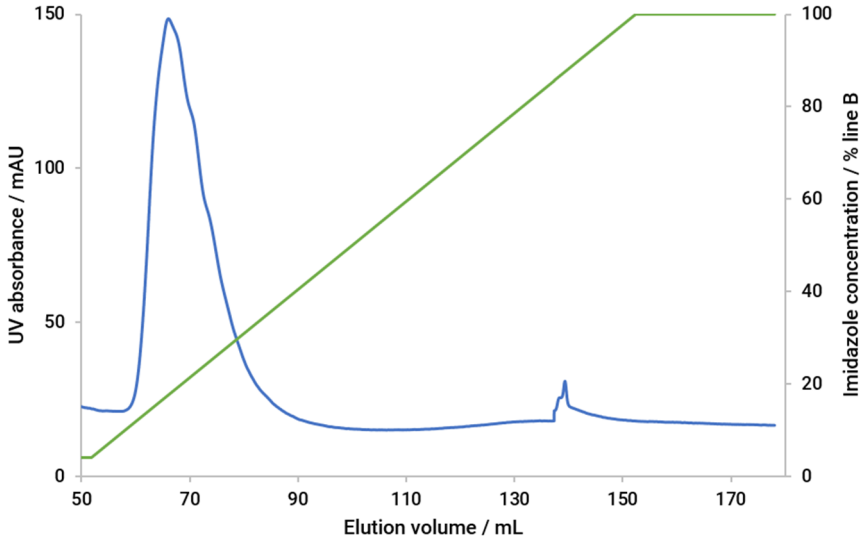


**Figure 5.6** Chromatogram of IMAC-purified ReLDIase using an ÄKTA start, expressed in 4 L LB media and lysed by pressure homogenisation. The UV absorbance is shown in blue, with the imidazole gradient in green.

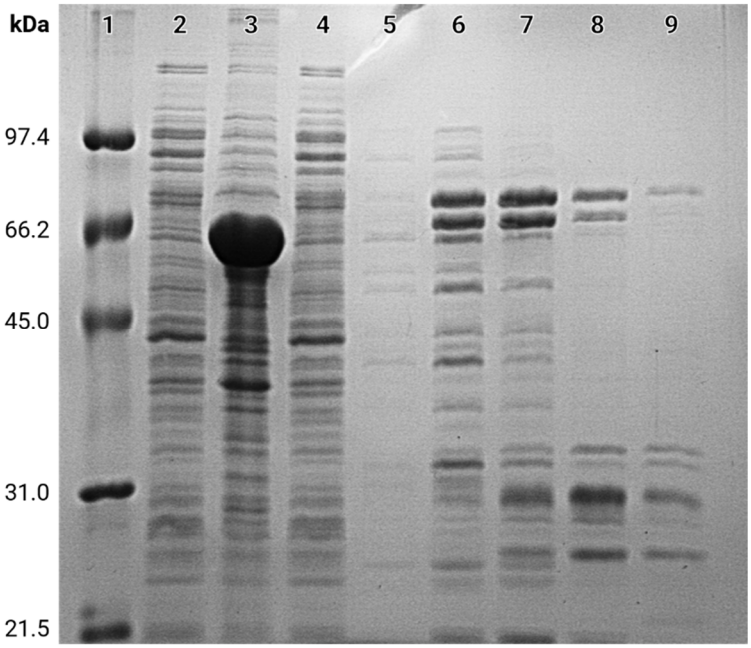


**Figure 5.7** SDS-PAGE of selected ReLDIase fractions from IMAC purification. Lane (1): low molecular weight marker; lane (2): clarified cell lysate; lane (3): insoluble fraction; lane (4): IMAC-purification wash; lanes (5-9): 5 mL fractions eluted by increasing imidazole concentration.

Both the chromatogram and SDS-PAGE analysis (***Figure 5.7***) showed no soluble expression of the gene of interest. The short peak on the chromatogram is likely to be non-specifically bound background protein. An alternative strategy for soluble ReLDIase expression to overcome these issues was investigated.

## 5.4. ReLDI-27ase

To improve solubility, a signal peptide was identified using SignalP, Technical University Denmark.

To remove this signal peptide, a forward primer was designed starting 81 bp into the ReLDIase gene to remove 27 amino acid residues from the N-terminus [***2.1.3***]. This truncated protein was named ReLDI-27ase.

For molecular cloning by LIC [***2.3***], this forward primer was used with the standard reverse primer of ReLDIase in a touchdown PCR reaction [***2.3.2***]. A band between 1.5-2 kb was excised and purified by gel extraction, followed by T4 polymerase treatment and annealing to linearised pET-YSBLIC3C vector (57 ng $\mu L^{-1}$) as for ReLDIase. Reactions were transformed into *E. coli* and used for colony PCR [***2.3.7***].

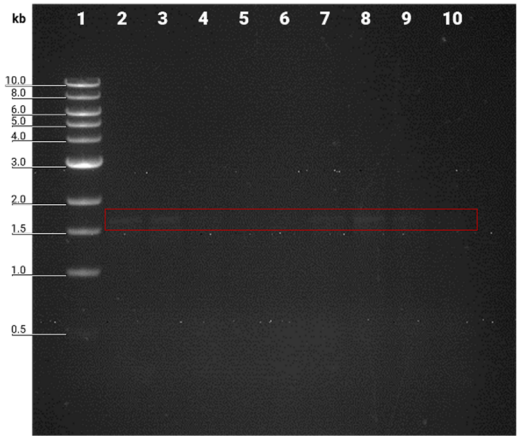


**Figure 5.8** An agarose gel of colony PCR to test the success of ReLDI-27ase gene cloning into pET-YSBLIC3C. Bands highlighted in red can be very faintly observed at ~1.7 kb, matching the insert size.

The agarose gel (***Figure 5.8***) showed bands of the correct size, yet were too faint to be conclusive. A double restriction digest using NcoI and NdeI was carried out using transformants of the ratios 1:5 and 5:1 gene insert to vector [***2.3.8***] (***Figure 5.9***). This digest showed clear bands matching the expected sizes for successful cloning; 5308 bp, 904 bp, 441 bp and 276 bp. The smallest band of 86 bp was not resolved, however due to its size this was expected.

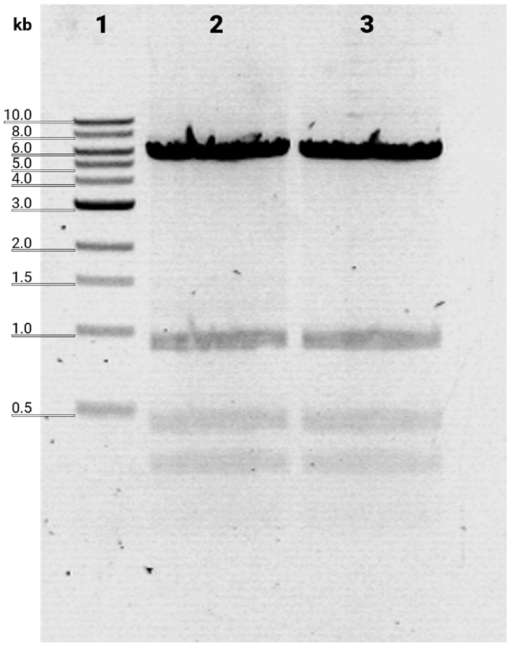


**Figure 5.9** A double restriction digest to test the success of ReLDI-27ase gene cloning into pET-YSBLIC3C. Four visible bands match expected fragment sizes of 5.3 kb, 0.9 kb, 0.4 kb and 0.3 kb.

## 5.5. ReLDI-27ase expression and purification

ReLDI-27ase was transformed into *E. coli* BL21(DE3) and large-scale expression in 1 L TB was carried out [***2.8***]. Cells were lysed by sonication and purified by IMAC on an ÄKTA pure [***2.10.1***] (***Figure 5.10***).

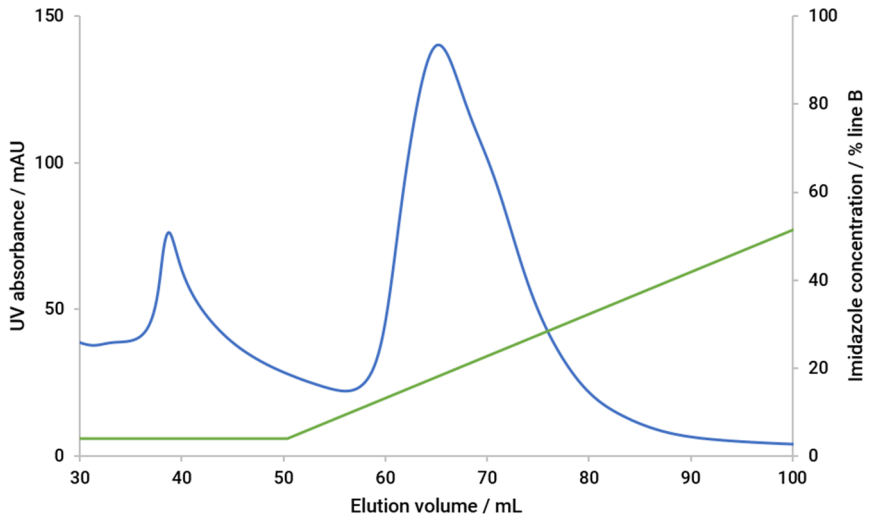


**Figure 5.10** Chromatogram of IMAC-purified ReLDI-27ase using an ÄKTA pure, expressed in 1 L TB media and lysed by sonication. The UV absorbance is shown in blue, with the imidazole gradient in green.

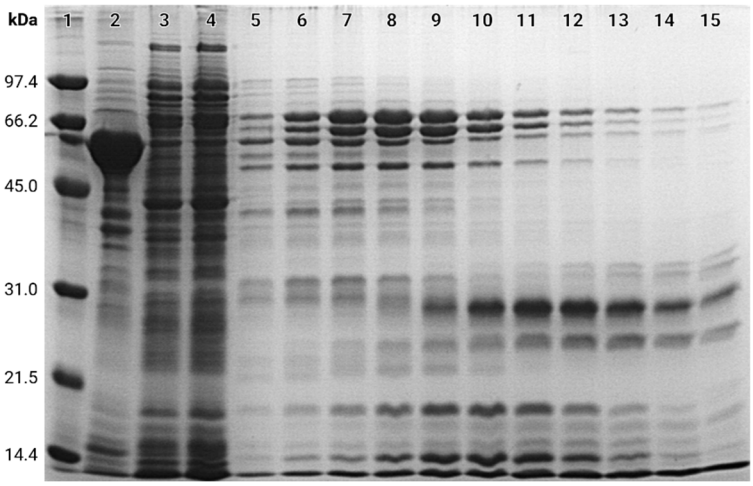


**Figure 5.11** SDS-PAGE of selected ReLDI-27ase fractions from IMAC purification. Lane (1): low molecular weight marker; lane (2): insoluble fraction; lane (3): clarified cell lysate; lane (4): HisTrap FF Crude column loading flow-through; lanes (5-15): 1.8 mL fractions eluted by increasing imidazole concentration.

Although a peak was visualised on the chromatogram, SDS-PAGE analysis (***Figure 5.11***) showed the protein of interest was missing in fractions, yet indicated insoluble expression.

## 5.6. ReLDI-27ase expression tests

Expression tests were carried out as the next step to determine whether varying conditions may improve soluble expression (***Figure 5.12***). The same growth media and induction temperatures were tested as for ReLDIase. Unfortunately, soluble expression was again not observed.

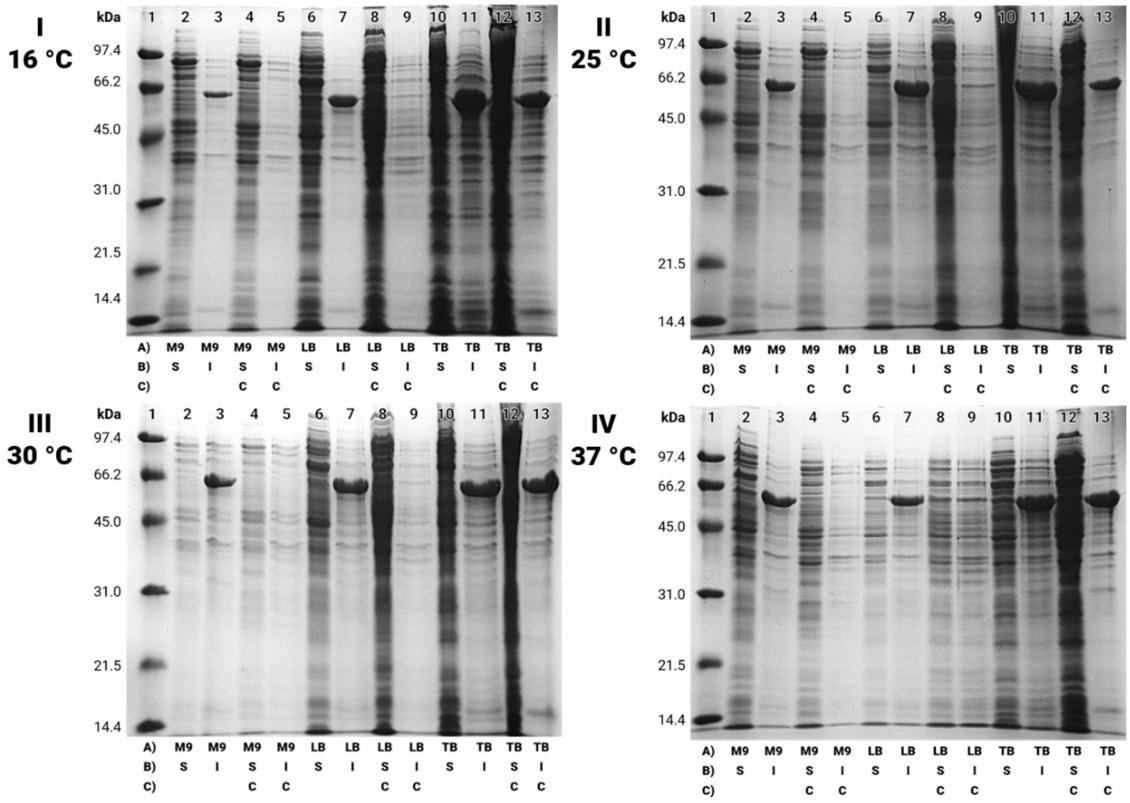


**Figure 5.12** ReLDI-27ase expression tests in *E. coli* BL21. Temperatures of induction are shown to the top right of each gel. A) denotes media; B) denotes soluble (S) or insoluble (I) fractions; C) denotes controls (C).

## 5.7. Conclusions

Although ReLDIase appeared a promising candidate for a LDIase homologue which would perform better under aerobic conditions, it did not demonstrate sufficient soluble expression for purification and crystallisation. For further investigation many strategies exist to potentially solve this problem, such as buffer screens during cell lysis or co-expression of chaperones. Alternatively, a C-terminal hexahistidine tag could be used by changing the cloning vector. Although these strategies were not possible during the time frame of this work, they may provide a solution to allow structural determination of this enzyme.

# Chapter 6.

## Discussion

The use of enzymes to enantioselectively add water across electron-rich carbon-carbon double bonds not only enriches the biocatalytic toolbox available to industry, but also allows for the conversion of cheap bio-derived feedstocks into fine chemicals to improve affordability and end our current reliance on petrochemical sources. Although enzymes exist which catalyse this reaction, they are limited by substrate range; oleate hydratase is *cis*-specific, acetylene hydratase is oxygen sensitive, and carotenoid hydratases are cofactor dependent.

Linalool Dehydratase-Isomerase (LDIase) may provide a solution to these constraints, in addition to providing dehydratase activity.[76] To take full advantage of this enzyme for industrial purposes the structure and mechanism must be understood, allowing rational design for a broad substrate range and maximal enantiomeric excess.

The prior structural characterisation of LDIase has provided insight into the mechanism of its dehydratase and isomerase functions. However, the mechanism for enantioselective hydration remains elusive. Through co-crystallisation and mutagenesis studies, this work has provided insight into how the enzyme achieves this and provides further evidence for a covalent intermediate. Parallel investigation of a homologue was attempted as a step towards identifying a mechanistic family of hydratases.

Co-crystallisation of LDIase aimed to yield a structure with ligand density for a linalool-bound complex, though this was not successful. However, possible methods for overcoming this may exist. The reasons for oxygen-sensitivity of the enzyme are not clear; it is possible this may be due to the proximal cysteines 171 and 180 forming a disulfide bridge under oxidative conditions. Further attempts using the reducing agent dithiothreitol (DTT) in

purification or crystallisation could provide such a complex. In conjunction, the co-crystallisation strategy successfully applied to the mutant may be similarly effective in this case.

The aerobic homologue ReLDIase was successfully cloned into the LIC3C vector, though unfortunately the expressed protein was insoluble under a range of conditions. Additional strategies can be taken in future work to enable soluble expression of this protein.

Mutagenesis of the LDIase cysteine residue 171 to serine allowed for structural analysis of its role in the catalytic mechanism. Extraneous electron density was observed in the active site which, although not sufficient to be a ligand-complex, could indicate a covalent bond to C180. H129 is also located proximally to this density, further suggesting its catalytic importance. Further mutagenesis of C171 to an alanine could shed further light on this mechanism by removing the side chain altogether.

Overall, this work has demonstrated the difficult expression of a homologue ReLDIase, formed a reliable strategy for crystallisation of the protein LDIase, and provided further evidence through mutagenesis for the formation of a covalent intermediate in its mechanism. A pathway for subsequent experiments will allow for a complete mechanistic understanding of this novel hydration mechanism and its future rational design for industrial applications.

# Abbreviations

| | |
|---|---|
| APS | Ammonium persulfate |
| CV | Column volumes |
| DMSO | Dimethyl sulfoxide |
| IMAC | Immobilised Metal Affinity Chromatography |
| IPTG | Isopropyl β-D-thiogalactopyranoside |
| LC-MS | Liquid Chromatography-tandem Mass Spectrometry |
| LIC | Ligation Independent Cloning |
| LDIase | Linalool Dehydratase-Isomerase |
| M9 | Minimal media 9 |
| PAGE | Polyacrylamide gel electrophoresis |
| PCR | Polymerase Chain Reaction |
| ReLDIase | *Rhodococcus erythropolis* Linalool Dehydratase-Isomerase |
| ReLDI-27ase | *R. erythropolis* Linalool Dehydratase-Isomerase, *sans* signal peptide |
| SDS | Sodium dodecyl sulfate |
| SEC | Size Exclusion Chromatography |
| TAE | Tris-acetate-EDTA |
| TEMED | Tetramethylethylenediamine |
| Tris | Tris(hydroxymethyl)aminomethane |
| UPW | Type I ultrapure water (> 18 MΩ·cm) |

# References


[1] V. Resch, U. Hanefeld, *Catal. Sci. Technol.* ***2015***, *5*, 1385–1399.

[2] R. A. Britton, (Esso Research and Engineering Company), US 3686334 A, ***1972***.

[3] M. Sada, M. Kato, Y. Mori, M. Sano, (Sumitomo Chemical Company Limited), US 4307257 A, ***1981***.

[4] J. M. Dreiling, T. J. Gay, *Phys. Rev. Lett.* ***2014***, *113*, 1–5.

[5] R. Bentley, *Chem. Rev.* ***2006***, *106*, 4099–4112.

[6] I. Agranat, H. Caner, J. Caldwell, *Nat. Rev. Drug Discov.* ***2002***, *1*, 753–768.

[7] S. K. Teo, W. A. Colburn, W. G. Tracewell, K. A. Kook, D. I. Stirling, M. S. Jaworsky, M. A. Scheffler, S. D. Thomas, O. L. Laskin, *Clin. Pharmacokinet.* ***2004***, *43*, 311–327.

[8] C. D. Vanderwal, E. N. Jacobsen, *J. Am. Chem. Soc.* ***2004***, *126*, 14724–14725.

[9] E. Hartmann, D. J. Vyas, M. Oestreich, *Chem. Commun.* ***2011***, *47*, 7917–32.

[10] A. J. Boersma, D. Coquière, D. Geerdink, F. Rosati, B. L. Feringa, G. Roelfes, *Nat. Chem.* ***2010***, *2*, 991–995.

[11] L. Xue, B. Jia, L. Tang, X. F. Ji, M. Y. Huang, Y. Y. Jiang, *Polym. Adv. Technol.* ***2004***, *15*, 346–349.

[12] S. Wang, Z. Zhang, C. Chi, G. Wu, J. Ren, Z. Wang, M. Huang, Y. Jiang, *React. Funct. Polym.* ***2008***, *68*, 424–430.

[13] G. J. Bartlett, C. T. Porter, N. Borkakoti, J. M. Thornton, *J. Mol. Biol.* ***2002***, *324*, 105–121.

[14] B. M. Nestl, S. C. Hammer, B. A. Nebel, B. Hauer, *Angew. Chemie - Int. Ed.* ***2014***, *53*, 3070–3095.

[15] R. J. Sowden, S. Yasmin, N. H. Rees, S. G. Bell, L.-L. Wong, *Org. Biomol. Chem.* ***2005***,

*3*, 57–64.

[16] L.-L. Wong, S. G. Bell, A. B. Carmichael, (Isis Innovation Limited), WO 2000031273 A2, ***2000***.

[17] S. K. Ma, J. Gruber, C. Davis, L. Newman, D. Gray, A. Wang, J. Grate, G. W. Huisman, R. a. Sheldon, *Green Chem.* ***2010***, *12*, 81.

[18] C. K. Savile, J. M. Janey, E. C. Mundorff, J. C. Moore, S. Tam, W. R. Jarvis, J. C. Colbeck, A. Krebber, F. J. Fleitz, J. Brands, *et al.*, *Science* ***2010***, *329*, 305–309.

[19] U. T. Bornscheuer, G. W. Huisman, R. J. Kazlauskas, S. Lutz, J. C. Moore, K. Robins, *Nature* ***2012***, *485*, 185–194.

[20] A. M. Klibanov, *Nature* ***2001***, *409*, 241–246.

[21] D. Ro, E. M. Paradise, M. Ouellet, K. J. Fisher, K. L. Newman, J. M. Ndungu, K. A. Ho, R. A. Eachus, T. S. Ham, J. Kirby, *et al.*, *Nature* ***2006***, *440*, 3–6.

[22] J. D. Keasling, V. Martin, D. Pitera, S. T. Withers, J. Newman, (The Regents of the University of California), US 7192751 B2, ***2007***.

[23] K. J. Fisher, D. McPhee, F. X. Woolard, (Amyris Biotechnologies Inc.), WO 2009088404 A1, ***2009***.

[24] L. A. Laffend, V. Nagarajan, C. E. Nakamura, (E I Du Pont de Nemours and Company), US 5686276 A, ***1997***.

[25] D. M. Adkesson, A. W. Alsop, T. T. Ames, L. A. Chu, J. M. Disney, B. C. Dravis, P. Fitzgibbon, J. M. Gaddy, F. G. Gallagher, W. F. Lehnhardt, *et al.*, (E I Du Pont de Nemours and Company), US 20050069997 A1, ***2005***.

[26] N. E. Drysdale, F. Nederberg, (E I Du Pont de Nemours and Company), US 20130005922 A1, ***2013***.

[27] D. H. Flint, M. H. Emptage, J. R. Guest, *Biochemistry* ***1992***, *31*, 10331–10337.

[28] D. H. Flint, *Arch. Biochem. Biophys.* ***1994***, *311*, 509–516.

[29] P. R. Feliciano, C. L. Drennan, M. C. Nonato, *Proc. Natl. Acad. Sci.* ***2016***, *1*, 201605031.

[30] I. A. Rose, T. M. Weaver, *Proc. Natl. Acad. Sci. U. S. A.* ***2004***, *101*, 3393–7.

[31] A. E. Mechaly, A. Haouz, I. Miras, N. Barilone, P. Weber, W. Shepard, P. M. Alzari, M. Bellinzoni, *FEBS Lett.* ***2012***, *586*, 1606–1611.

[32] M. Mescam, K. C. Vinnakota, D. A. Beard, *J. Biol. Chem.* ***2011***, *286*, 21100–21109.

[33] C. P. Tseng, C. C. Yu, H. H. Lin, C. Y. Chang, J. T. Kuo, *J. Bacteriol.* ***2001***, *183*, 461–467.

[34] Z. Chi, Z.-P. Wang, G.-Y. Wang, I. Khan, Z.-M. Chi, *Crit. Rev. Biotechnol.* ***2014***, *8551*, 1–9.

[35] T. Weaver, M. Lees, V. Zaitsev, I. Zaitseva, E. Duke, P. Lindley, S. McSweeny, a Svensson, J. Keruchenko, I. Keruchenko, *et al.*, *J. Mol. Biol.* ***1998***, *280*, 431–442.

[36] C. K. Engel, M. Mathieu, J. P. Zeelen, J. K. Hiltunen, R. K. Wierenga, *Embo J* ***1996***, *15*, 5135–5145.

[37] J. K. Hiltunen, Y. M. Qin, *Biochim. Biophys. Acta - Mol. Cell Biol. Lipids* ***2000***, *1484*, 117–128.

[38] B. J. Bahnson, V. E. Anderson, G. A. Petsko, *Biochemistry* ***2002***, *41*, 2621–2629.

[39] X. Cui, R. He, Q. Yang, W. Shen, M. Li, *J. Mol. Model.* ***2014***, *20*, 1–12.

[40] R. B. Hamed, E. T. Batchelar, I. J. Clifton, C. J. Schofield, *Cell. Mol. Life Sci.* ***2008***, *65*, 2507–2527.

[41] T. Fukui, Naofumi Shiomi, Y. Doi, *J. Bacteriol.* ***1998***, *180*, 667–673.

[42] M. Kristian Koski, A. M. Haapalainen, J. K. Hiltunen, T. Glumoff, *J. Mol. Biol.* ***2005***, *345*, 1157–1169.

[43] T. J. K. Haataja, M. K. Koski, J. K. Hiltunen, T. Glumoff, *Biochem. J.* ***2011***, *435*, 771–81.

[44] P. Kasaragod, W. Schmitz, J. K. Hiltunen, R. K. Wierenga, *FEBS J.* ***2013***, *280*, 3160–3175.

[45] S. Sato, C. T. Nomura, H. Abe, Y. Doi, T. Tsuge, *J. Biosci. Bioeng.* ***2007***, *103*, 38–44.

[46] A. Marx, M. Poetter, S. Buchholz, A. May, H. Siegert, B. Alber, G. Fuchs, L. Eggeling, (Evonik Roehm Gmbh), US 20100291644 A1, ***2010***.

[47] A. P. Burgard, P. Pharkya, R. E. Osterhout, (Genomatica Inc.), US 20090305364 A1, ***2009***.

[48] C. Bessler, J. Feesche, S. Evers, K.-H. Maurer, A. Ehrenreich, B. Veith, H. Liesegang, A. Henne, C. Herzberg, G. Gottschalk, US 20070190605 A1, ***2007***.

[49] E. N. Davis, L. L. Wallen, J. C. Goodwin, W. K. Rohwedder, *Lipids* ***1969***, *4*, 356–362.

[50] L. E. Bevers, M. W. H. Pinkse, P. D. E. M. Verhaert, W. R. Hagen, *J. Bacteriol.* ***2009***, *191*, 5010–5012.

[51] M. Engleder, T. Pavkov-Keller, A. Emmerstorfer, A. Hromic, S. Schrempf, G. Steinkellner, T. Wriessnegger, E. Leitner, G. A. Strohmeier, I. Kaluzna, *et al.*, *ChemBioChem* ***2015***, *16*, 1730–1734.

[52] S. Gocho, N. Tabogami, M. Inagaki, C. Kawabata, T. Komai, *Biosci. Biotechnol. Biochem.* ***1995***, *59*, 1571–1572.

[53] A. Wanikawa, K. Hosoi, I. Takise, T. Kato, *J. Inst. Brew.* ***2000***, *106*, 39–43.

[54] J. U. An, Y. C. Joo, D. K. Oh, *Appl. Environ. Microbiol.* ***2013***, *79*, 2636–2641.

[55] A. Hiseni, I. W. C. E. Arends, L. G. Otten, *Appl. Microbiol. Biotechnol.* ***2011***, *91*, 1029–1036.

[56] A. Hiseni, L. G. Otten, I. W. C. E. Arends, *Appl. Microbiol. Biotechnol.* ***2016***, *100*, 1275–1284.

[57] D. V Spracklen, B. Bonn, K. S. Carslaw, *Philos. Trans. A. Math. Phys. Eng. Sci.* ***2008***, *366*,

4613–26.

[58] M. Ligor, M. Stankevičius, A. Wenda-Piesik, K. Obelevičius, O. Ragažinskienė, Ž. Stanius, A. Maruška, B. Buszewski, *Food Anal. Methods* ***2013***, *7*, 1433–1442.

[59] M. L. Thompson, R. Marriott, A. Dowle, G. Grogan, *Appl. Microbiol. Biotechnol.* ***2010***, *85*, 721–730.

[60] M. B. Kolicheski, L. C. Cocco, D. A. Mitchell, M. Kaminski, *J. Anal. Appl. Pyrolysis* ***2007***, *80*, 92–100.

[61] W. Chen, A. M. Viljoen, *South African J. Bot.* ***2010***, *76*, 643–651.

[62] K. Ebel, F. Funke, T. Gerlach, H.-G. Gobbel, R. Korner, L. Lobree, E. Schwab, S. Unverricht, (BASF Ag), EP 1317959 A1, ***2003***.

[63] F. Funke, T. Gerlach, M. Haake, (BASF Ag), EP 1318129 A2, ***2003***.

[64] A. C. Aprotosoaie, M. Hăncianu, I. I. Costache, A. Miron, *Flavour Fragr. J.* ***2014***, *29*, 193–219.

[65] M. Matura, M. Sköld, A. Börje, K. E. Andersen, M. Bruze, P. Frosch, A. Goossens, J. D. Johansen, C. Svedman, I. R. White, *et al.*, *Contact Dermatitis* ***2005***, *52*, 320–328.

[66] J.-M. Chantraine, J.-M. Dhenin, C. Moretti, *J. Essent. Oil Res.* ***2009***, *21*, 486–496.

[67] S. Ulland, E. Ian, A. K. Borg-Karlson, H. Mustaparta, *Chem. Senses* ***2006***, *31*, 325–334.

[68] F. Chen, D. Tholl, J. Bohlmann, E. Pichersky, *Plant J.* ***2011***, *66*, 212–229.

[69] R. Marmulla, J. Harder, *Front. Microbiol.* ***2014***, *5*, 1–14.

[70] Z. Zebec, J. Wilkes, A. J. Jervis, N. S. Scrutton, E. Takano, R. Breitling, *Curr. Opin. Chem. Biol.* ***2016***, *34*, 37–43.

[71] D. Brodkorb, M. Gottschall, R. Marmulla, F. Lüddeke, J. Harder, *J. Biol. Chem.* ***2010***, *285*, 30436–30442.

[72] S. Foss, U. Heyen, J. Harder, *Syst. Appl. Microbiol.* ***1998***, *21*, 237–244.

[73] P. Kämpfer, K. Denger, A. M. Cook, S. T. Lee, U. Jäckel, E. B. M. Denner, H. J. Busse, *Int. J. Syst. Evol. Microbiol.* ***2006***, *56*, 815–819.

[74] F. Lüddeke, J. Harder, *Zeitschrift fur Naturforsch. - Sect. C J. Biosci.* ***2011***, *66 C*, 409–412.

[75] B. M. Nestl *et al., Nat. Chem. Biol.* ***2017*** in press.

[76] P. Marliere, (Scientist of Fortune SA), US 8703455 B2, ***2014***.

[77] P. Marliere, (Scientist of Fortune SA), WO 2014033129 A1, ***2014***.

[78] P. Marliere, M. Delcourt, S. Mazaleyrat, (Scientist of Fortune SA), WO 2014184345 A1, ***2014***.

[79] H. Mooibroek, K. Cornish, *Appl. Microbiol. Biotechnol.* ***2000***, *53*, 355–365.

[80] N. Martins, F. Bonnet, M. Visseaux, *Polym. (United Kingdom)* ***2014***, *55*, 5013–5016.

[81] F. Fisch, C. M. Fleites, M. Delenne, N. Baudendistel, B. Hauer, J. P. Turkenburg, S. Hart, N. C. Bruce, G. Grogan, *J. Am. Chem. Soc.* ***2010***, *132*, 11455–11457.

[82] D. J. Korbie, J. S. Mattick, *Nat. Protoc.* ***2008***, *3*, 13–15.

[83] M. J. Fogg, A. J. Wilkinson, *Biochem. Soc. Trans.* ***2008***, *36*, 771–775.

[84] D. Hanahan, *J. Mol. Biol.* ***1983***, *166*, 557–580.

[85] S. Panja, P. Aich, B. Jana, T. Basu, *Mol. Membr. Biol.* ***2008***, *25*, 411–422.

[86] W. Kabsch, *Acta Crystallogr. Sect. D Biol. Crystallogr.* ***2010***, *66*, 125–132.

[87] P. Evans, *Acta Crystallogr. Sect. D Biol. Crystallogr.* ***2006***, *62*, 72–82.

[88] G. Winter, *J. Appl. Crystallogr.* ***2010***, *43*, 186–190.

[89] A. Vagin, A. Teplyakov, *J. Appl. Cryst* ***1997***, *30*, 1022–1025.

[90] P. Emsley, K. Cowtan, *Acta Crystallogr. Sect. D Biol. Crystallogr.* ***2004***, *60*, 2126–2132.

[91] G. N. Murshudov, A. A. Vagin, E. J. Dodson, *Acta Crystallogr. Sect. D Biol. Crystallogr.* ***1997***, *53*, 240–255.

[92] A. M. Hassell, G. An, R. K. Bledsoe, J. M. Bynum, H. L. Carter, S. J. J. Deng, R. T. Gampe, T. E. Grisard, K. P. Madauss, R. T. Nolte, *et al.*, *Acta Crystallogr. Sect. D Biol. Crystallogr.* ***2006***, *63*, 72–79.